



## Control oriented model-based simulation and experimental studies on a compliant legged quadruped robot<sup>☆</sup>

M.M. Gor<sup>a</sup>, P.M. Pathak<sup>a,\*</sup>, A.K. Samantaray<sup>b</sup>, J.-M. Yang<sup>c</sup>, S.W. Kwak<sup>d</sup>

<sup>a</sup> Indian Institute of Technology Roorkee, India

<sup>b</sup> Indian Institute of Technology Kharagpur, India

<sup>c</sup> Kyungpook National University, Daegu, South Korea

<sup>d</sup> Keimyung University, Daegu, South Korea



### HIGHLIGHTS

- Paper presents three dimensional dynamic model of quadruped with compliant legs.
- Model is verified with simulation, animation and experiment results.
- Turning motion is demonstrated by providing differential leg tip velocity.
- Influence of leg compliance on quadruped locomotion is studied.
- Energy efficient structure, gait and foot trajectory have been carried out.

### ARTICLE INFO

#### Article history:

Received 24 September 2014

Received in revised form

21 May 2015

Accepted 9 June 2015

Available online 17 June 2015

#### Keywords:

Quadruped robot

Bond graph

Dynamic model

Compliant leg

Locomotion gait

Foot trajectory

### ABSTRACT

Quadruped robots offer better maneuverability over wheeled mobile robots. However, a quadruped robot contains many joint actuators which have to operate in a coordinated fashion to achieve the desired locomotion. Joint actuations cause various degrees of disturbance on the robot body and may even destabilize the system. Thus, prior dynamic analysis plays an important role for development of control laws for quadruped locomotion. Here, a three dimensional dynamic model of a quadruped has been developed using the bond graph technique which can be interfaced with various controller models. This model contains a detailed sub-model for telescopic compliant legs. Results from simulations, animations and experiments are discussed. Turning motion at various leg speeds is studied for dynamic stability of the robot. The effect of leg compliance on locomotion parameters is studied which helps in selecting a suitable compliance. Performance measure is carried out using energy efficiency as deciding criteria. Study on energy efficient quadruped structure, energy efficient locomotion gait and foot trajectory have been carried out for designing an efficient quadruped.

© 2015 Elsevier B.V. All rights reserved.

### 1. Introduction

Legged robot offers many advantages over wheeled robots including greater adaptability to terrain irregularities and superior off-road mobility [1,2]. Legged systems require only a series of discrete footholds along the pathway for off-road locomotion. This

property enables legged robots to traverse surfaces inaccessible to wheeled mobile robots. Compliance in the leg improves locomotion of legged robot [3]. Variable compliance in the legs [4] overcomes the size, weight, fragility and efficiency problem. Basically, legged robots are discrete systems in which joints of each leg have to operate in particular fashion. So, dynamics plays an important role in the operation and control of a walking robot. Recently, there has been a noteworthy increase in the use of computational dynamics for design, analysis, simulation and control of various robotic systems. This is due to availability of various multi-body dynamic analysis tools and faster computational resources. To this end, various researchers used different dynamic analysis methods for multi-body systems, such as the methods based on Lagrangian

<sup>☆</sup> A part of this paper has been published in 1st International and 16th National Conference on Machines and Mechanisms (iNaCoMM 2013) held at IIT Roorkee, India from December 18–20, 2013.

\* Corresponding author.

E-mail addresses: [mehulmgor@gmail.com](mailto:mehulmgor@gmail.com) (M.M. Gor), [pushpfme@iitr.ac.in](mailto:pushpfme@iitr.ac.in) (P.M. Pathak), [samantaray@mech.iitkgp.ernet.in](mailto:samantaray@mech.iitkgp.ernet.in) (A.K. Samantaray), [jmyang@ee.knu.ac.kr](mailto:jmyang@ee.knu.ac.kr) (J.-M. Yang), [ksw@kmu.ac.kr](mailto:ksw@kmu.ac.kr) (S.W. Kwak).

equation [5], Newton–Euler equation [6,7], Kane's equation [8–10] and variational methods [11].

Bennani and Giri [12] presented a dynamic model approach of quadruped considering open and/or closed kinematic chain mechanisms. It is based on Newton–Euler approach and the explicit formulation of kinematic holonomic constraints for the closed loop mechanism. Mahapatra and Roy [13] developed a dynamic model of six legged in CATIA solid modeler, SimDesigner and ADAMS multi-body dynamic solver and kinematic and dynamic simulation is performed based on virtual prototyping technology. Krishnan et al. [14] presented a bond graph model of compliant legged quadruped robot in a sagittal plane. The sagittal plane dynamics have been tested through experimental set-up. Soyguder and Ali [15] solved the stance and flight phase dynamic structures in a sequential closed loop for quadruped and obtained the equation of motion for pronking gait. Shah et al. [16] presented a concept of kinematic modules for the development of the dynamic model of the four legged robots where each module is considered as a set of serially connected links. Module-level Decoupled Natural Orthogonal Complement (DeNOC) matrices were introduced which helps to analyze the large number of links as a system with a smaller number of modules. Recursive kinematic relationships were obtained between two adjoining modules. Ganesh and Pathak [17] developed a dynamic model of four legged in a sagittal plane by formulating kinetic and potential energy equation of body and leg. These were used to derive Lagrangian function and then equation of motion. A locomotion control strategy for a quadruped robot has been presented in [18]. Dynamic modeling and analysis of quadruped robot through bond graph technique has been presented in [19].

Many of the quadruped robots developed worldwide are biologically inspired. Process of natural selection governing evolution of species forces animals adapt to their specific physical features and environment by optimizing their locomotion. Some animals are better at doing certain things in comparison to others. Thus, keeping the required task or operation features in the view, more and more specialized biologically inspired quadrupeds are being developed now-a-days. Some of them are Baby Elephant [20], BigDog [21], Cheetah-cub [22], HyQ [23], LittleDog [24,25] and Tekken [26,27]. Hydraulically actuated Baby Elephant [20] was designed to work as mechanical carrier. It has 12 DOFs and compliant legs. Multi-body dynamic simulation was used in [20] for its design and the results were experimentally validated. BigDog [21] was developed with the goal to move in rough terrain without human assistance. It has twenty DOFs and about fifty sensors. Four joints of each leg are operated by hydraulic actuator. It uses a two-stroke internal combustion engine that delivers up to 15 hp power. Electrically actuated Cheetah-cub [22] was designed for high-speed locomotion. Cheetah-cub's legs are spring loaded and pantograph mechanism with multiple segments is used for shock absorption during running. This robot's self-stabilizing properties were demonstrated in hardware model and in simulation carried out in Webots software. HyQ [23] developed at IIT Genova was designed to perform highly dynamic tasks like jumping and running. It has 12 DOFs and both hydraulic and electrical actuation systems. During running and jumping, generated impact forces were absorbed by hydraulic actuation mounted on hip and knee joints in the flexion/extension plane of the leg. The hip abduction/adduction joint was actuated by brushless electric motor which provides constant output torque. LittleDog [24,25] has 12 DOFs and each joint is operated by a high-gain servo motor. Sensors mounted on the robot measure body orientation, joint angles and ground-foot contact. Sensing, communication and actuators are controlled by onboard PC-level computer. Tekken [26,27] is a light weight (4.3 kg) manually operated power autonomous compliant legged quadruped robot. It has 16 DOFs, 3 joints around pitch axis (ankle,

knee and hip) and 1 hip joint around yaw axis at each leg. At ETH Zurich, two quadrupeds have been developed having similar structure, size, and morphology, but different concept of actuation [28]. The first, ALoF, is a classically stiff actuated robot that is controlled kinematically; whereas the second, StarlETH, uses a soft actuation scheme based on highly compliant series elastic actuators.

In this paper, three dimensional dynamic model of compliant legged quadruped robot using bond graph has been developed. Bond graph technique is a graphical tool presenting the energy exchange between elements representing the model properties. It is a common language to model any systems involving different energetic domains. It clearly shows the cause and effect relations in the model. Structural properties of the system can be also analyzed using bond graph. Controller model can be integrated with bond graph model and physical model-based control laws can be designed with it. These are the few reasons to choose bond graph as modeling tool. A quadruped robot configuration used for analysis is two links legged robot in which upper link is rigid and a lower link is compliant. Lower link is considered similar to a prismatic link in which, piston and piston rod is sliding inside the cylinder and movement is restricted by the spring which generates compliance in the leg. To validate the developed model, simulation and animation of the trot gait performed by the quadruped is carried out which is further verified by experiment results. Since trot gait is dynamically stable gait thus successful validation of model in trot gait ensures the model validity in other gaits also. To prove the versatility of the three dimensional model generated a turning motion of the robot is demonstrated by varying the leg speed in amble gait. Influence of compliance on quadruped locomotion and posture disturbance is studied. Performance analysis is carried out considering energy efficiency as deciding criteria. Performance analysis on rigid and compliant legged robots, static and dynamic gaits, and foot trajectory are carried out. A part of this work is published in [19].

This paper is organized in the following sequence. In Section 2, three dimensional dynamic model of quadruped robot is developed using bond graph. Dynamics of body and leg is discussed in detail. In Section 3, simulation, animation and experiment results of trot gait are discussed. In this section, turning motion of the quadruped robot, influence of compliance on locomotion and performance measure of various quadruped aspects by energy efficiency is also discussed. Section 4 concludes this paper.

## 2. Modeling of a quadruped robot

Modeling of a quadruped robot consists of modeling of angular and translational dynamics of robot body and legs. Fig. 1(a) shows physical model of quadruped robot, while Fig. 1(b) shows the schematic diagram of a quadruped robot model in which {A} is an inertial frame and {B} is the body frame attached to body center of gravity (CG). Frame {0} is fixed at the hip joint of each leg which is fixed on the robot body. Each leg of the quadruped robot has two degree of freedom (DOF) with two revolute joints per leg. The joint between links  $i$  and  $i + 1$  is numbered as  $i + 1$ . A coordinate frame  $\{i + 1\}$  is attached to  $(i + 1)$  joint. Frame {1} is attached to joint 1 of each leg. Frame {0} is coinciding with frame {1}. Frame {2} is attached to joint {2}, while frame {3} is attached to leg tip. The rotational inertias are defined about frames fixed at the CG of the link. The CG frame is fixed along the principal directions in the link or body. The surface on which the robot is walking is assumed as a hard surface.

### 2.1. Dynamics of a robot body

For a given instant, any rigid body has absolute translational velocity  $\vec{v}$  and absolute angular velocity  $\vec{\omega}$ . The translational velocity and angular velocity vectors have been resolved into three

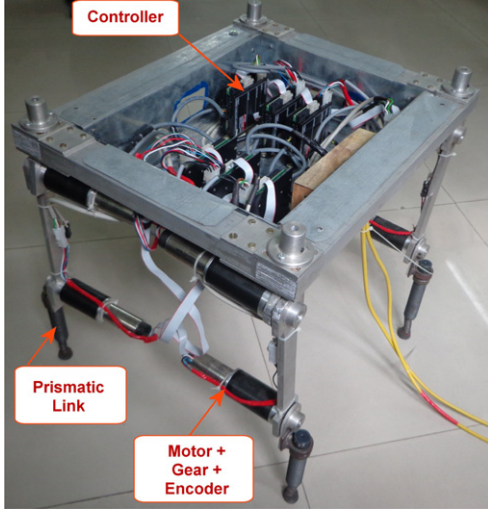


**Fig. 1(a).** Physical model of quadruped robot.

mutually perpendicular components  $v_x, v_y, v_z$  and  $\omega_x, \omega_y, \omega_z$ . The net force  $\vec{F}$  acting on the body and the linear momentum  $\vec{p}$  can be related with respect to rotating frame as [29],

$$\vec{F} = \left( \frac{\partial \vec{p}}{\partial t} \right)_{rel} + \vec{\omega} \times \vec{p} \quad (1)$$

where  $\left( \frac{\partial \vec{p}}{\partial t} \right)_{rel}$  is the rate of change of momentum relative to the moving frame. Similarly, the relationship between the net torque  $\vec{\tau}$  acting on the body and the angular momentum  $\vec{h}$  can be written as,

$$\vec{\tau} = \left( \frac{\partial \vec{h}}{\partial t} \right)_{rel} + \vec{\omega} \times \vec{h}. \quad (2)$$

Using the right-hand rule for Eqs. (1) and (2), the component equations can be written as,

$$F_x = m_b \dot{v}_x + m_b \omega_y v_z - m_b \omega_z v_y \quad (3)$$

$$F_y = m_b \dot{v}_y + m_b \omega_z v_x - m_b \omega_x v_z \quad (4)$$

$$F_z = m_b \dot{v}_z + m_b \omega_x v_y - m_b \omega_y v_x \quad (5)$$

and

$$\tau_x = I_{xb} \dot{\omega}_x + (I_{zb} - I_{yb}) \omega_y \omega_z \quad (6)$$

$$\tau_y = I_{yb} \dot{\omega}_y + (I_{xb} - I_{zb}) \omega_z \omega_x \quad (7)$$

$$\tau_z = I_{zb} \dot{\omega}_z + (I_{yb} - I_{xb}) \omega_x \omega_y. \quad (8)$$

These nonlinear differential equations are known as Newton–Euler's equations [30]. The cross product terms can be treated as forces in a set of Eqs. (3)–(5) and as torques in a set of Eqs. (6)–(8). The forces and torques can be added at the respective 1-junctions and using gyrator-ring structures bond graph is generated as presented in [30]. Generated structure is known as Euler Junction Structures (EJS).

## 2.2. Dynamics of a upper link of leg

Translational velocity of frame {0} of each leg with reference to frame {A} and expressed in terms of frame {A} is given by [31],

$${}^A(\vec{V}_0) = {}^A(\vec{V}_B) + {}_B R \left[ - {}^B(\vec{P}_0) \times {}^B(\vec{\omega}_B) \right] \quad (9)$$

where  ${}^A(\vec{V}_B)$  represents the translational velocity of body frame {B} with respect to an inertial frame {A} and expressed in frame

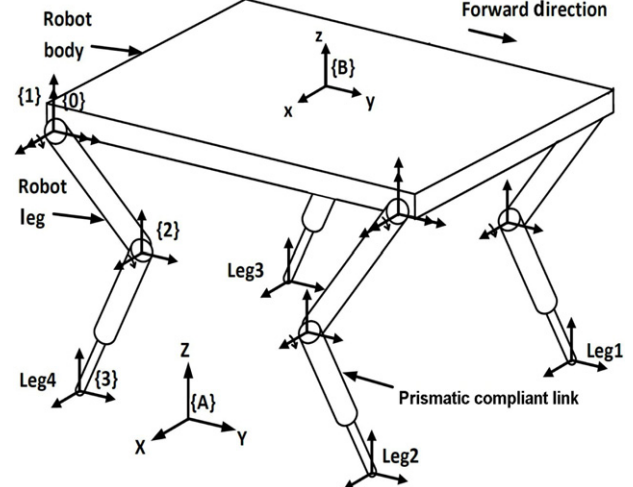


**Fig. 1(b).** Schematic representation of quadruped robot with compliant legs [19].

{A};  ${}^B(\vec{\omega}_B)$  represents the angular velocity of body frame {B} with respect to inertial frame {A} and expressed in frame {B};  ${}^B(\vec{P}_0)$  represents the position vector of frame {0} of ith leg with respect to the body CG frame {B} and expressed in frame {B}. It can be expressed as  ${}^B(\vec{P}_0)_i = [r_{ix} \ r_{iy} \ r_{iz}]^T$ , where 'i' denotes legs 1–4. Here  $r$  denotes position of frame {0} with respect to body CG frame. In Eq. (9),  ${}_B R$  represents the transformation from body frame {B} to inertial frame {A} and can be expressed as,

$${}^A R = \begin{pmatrix} c\theta c\phi & s\psi s\theta c\phi - c\psi s\phi & c\psi s\theta c\phi + s\psi s\phi \\ c\theta s\phi & s\psi s\theta c\phi + c\psi c\phi & c\psi s\theta s\phi - s\psi c\phi \\ -s\theta & s\psi c\theta & c\psi c\theta \end{pmatrix} \quad (10)$$

where  $c\theta$  is shorthand for  $\cos \theta$ ,  $s\theta$  for  $\sin \theta$  and so on.  $\phi$ ,  $\theta$  and  $\psi$  are the Z–Y–X Euler angles. Governing equation for an angular velocity propagation (AVP) of links of a leg can be given as [31],

$${}^{i+1}({}^A\vec{\omega}_{i+1}) = {}^{i+1}{}_i R {}^i({}^A\vec{\omega}_i) + {}^{i+1}({}^i\vec{\omega}_{i+1}) \quad (11)$$

where  ${}^{i+1}({}^A\vec{\omega}_{i+1})$  is the angular velocity of ( $i+1$ ) link with respect to inertial frame {A} and expressed in ( $i+1$ )th frame,  ${}^i({}^A\vec{\omega}_i)$  is the angular velocity of the  $i$ th link with respect to the inertial frame {A} and expressed in  $i$ th frame and  ${}^{i+1}({}^i\vec{\omega}_{i+1})$  is the angular velocity of ( $i+1$ ) link as observed from  $i$ th link and expressed in ( $i+1$ )th frame. The term can be expressed for links 1 and 2 respectively as,  ${}^1(\vec{\omega}_1) = [\dot{\theta}_1 \ 0 \ 0]^T$ ,  ${}^2(\vec{\omega}_2) = [\dot{\theta}_2 \ 0 \ 0]^T$ , where  $\dot{\theta}_1$  represents angular velocity of frame {1} with respect to frame {0} expressed in frame {1} and similarly  $\dot{\theta}_2$  represents the angular velocity of frame {2} with respect to frame {1} expressed in frame {2}.

For translational velocity propagation (TVP), governing equation for the link tip velocity and link CG velocity are given as,

$${}^A(\vec{V}_{i+1}) = {}^A(\vec{V}_i) + {}_i R \left[ {}^i({}^A\vec{\omega}_i) \times {}^i(\vec{P}_{i+1}) \right] \quad (12)$$

where  ${}^A(\vec{V}_{i+1})$  represents the translational velocity of body frame  $i+1$  with respect to an inertial frame {A} and expressed in frame {A},  ${}^A(\vec{V}_i)$  represents the translational velocity of body frame  $i$  with respect to an inertial frame {A} and expressed in frame {A},  ${}^i(\vec{P}_{i+1})$  represents position of frame  $i+1$  with respect to frame  $i$  and expressed in frame {i}. Link lengths  $l_1$  and  $l_2$  are taken along the principal Y-axis of the links and hence represented in vector form as,  ${}^0\vec{P}_1 = [0 \ 0 \ 0]^T$ ,  ${}^1\vec{P}_2 = [0 \ l_1 \ 0]^T$ ,  ${}^2\vec{P}_3 = [0 \ l_2 \ 0]^T$ .

Eq. (12) can be simplified as,

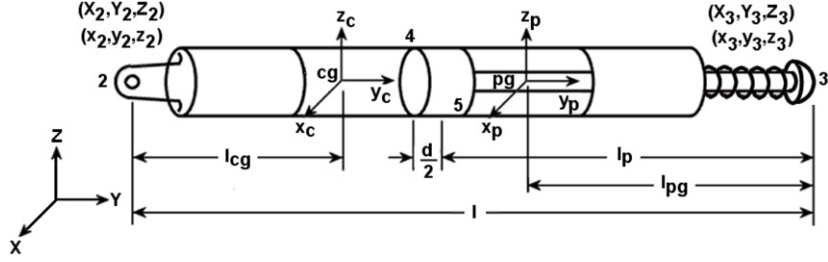


**Fig. 2.** Schematic diagram of prismatic link [34,35].

$${}^A(\vec{V}_{i+1}) = \left[ {}^A(\vec{V}_i) \right] + [{}^A R] \left[ -i (\vec{P}_{i+1}) \times \right] \left[ {}^i({}^A \vec{\omega}_i) \right]. \quad (13)$$

$$\text{For position of a link CG, } {}^i(\vec{P}_{Gi}) = [0 \quad l_{Gi} \quad 0]^T$$

$${}^A(\vec{V}_{Gi}) = \left[ {}^A(\vec{V}_i) \right] + [{}^A R] \left[ -i (\vec{P}_{Gi}) \times \right] \left[ {}^i({}^A \vec{\omega}_i) \right]. \quad (14)$$

Eqs. (12)–(14) represent the TVP of link in each leg of the robot. The CG velocity of links depends on link inertia. In the bond graph model “I” elements (representing mass of a link), are attached at flow junctions. They yield the CG velocities of links. The starting point of the current link is same as the previous link tip. Hence, the tip velocity of the previous link and the angular velocity of the current link are used to find the tip velocity and the CG velocity of the current link.  ${}^i({}^A \vec{\omega}_i)$  in above equations can be obtained from the AVP for the current link.

The EJS to represent angular dynamics of the link can be constructed similarly as discussed in Section 2.1. In case of link, torque is provided in x direction only. Nomenclature used throughout paper is listed in Appendix A.

### 2.3. Dynamics of the prismatic link

Lower link of the quadruped leg can be considered as a prismatic link, in which piston and piston rod is sliding inside cylinder. The movement is restricted by the internal hydraulic pressure of the cylinder and helical compression spring attached at the piston rod. This arrangement generates compliance in the leg. The sliding of piston is one of the most difficult multi body components which give rise to nonlinear equations of motion. It is important to develop bond graph model of prismatic link with proper mass distribution. Incorrect modeling of entire prismatic link generates improper inertial forces. Thus, utmost care should be taken at the time of generating bond graph model of the three dimensional prismatic link. Bond graph modeling of prismatic link is developed from the concept presented in [30,32–35]. The schematic drawing of prismatic link is shown in Fig. 2.

Local coordinate frame is attached at the center of mass of piston ( $x_p, y_p, z_p$ ) and cylinder ( $x_c, y_c, z_c$ ) and they are assumed to be aligned with the inertial principal axes. Piston and cylinder motions are described with reference to this body fixed coordinate system which rotate and translate with the respective rigid bodies. The end of the cylinder part will be fixed with the link 1 of quadruped robot and piston end will touch the ground.  $X_2, Y_2, Z_2$  and  $X_3, Y_3, Z_3$  are the inertial coordinate system while  $x_2, y_2, z_2$  and  $x_3, y_3, z_3$  are body fixed or non-inertial coordinate system of the cylinder and piston end respectively. The contemporary length  $l_c$  is the distance between the two end points. The center of gravity of the cylinder is located at a distance of  $l_{cg}$  from the fixed end. The combined center of gravity of the piston and the rod is located at a distance of  $l_{pg}$  from the rod end. The length of the piston is  $d$ . The center of the piston is located at a distance  $l_p$  from the rod end.

The velocity vector of the cylinder in the inertial frame is represented as  $\vec{v}_{xc, yc, zc}$  and in the body fixed frame as  $\vec{v}_{xc, yc, zc}$ . The angular velocity vector in the body fixed frame is  $\vec{\omega}_{xc, yc, zc}$ . Then, Euler equation for translatory motion of the cylinder can be given as,

$$F_{xc} = M_c \ddot{x}_c + M_c (\dot{z}_c \omega_{yc} - \dot{y}_c \omega_{zc}) \quad (15)$$

$$F_{yc} = M_c \ddot{y}_c + M_c (\dot{x}_c \omega_{zc} - \dot{z}_c \omega_{xc}) \quad (16)$$

$$F_{zc} = M_c \ddot{z}_c + M_c (\dot{y}_c \omega_{xc} - \dot{x}_c \omega_{yc}) \quad (17)$$

where  $F_{xc}, F_{yc}, F_{zc}$  are external forces acting in body-fixed  $x_c, y_c$  and  $z_c$  directions respectively,  $\omega_{xc}, \omega_{yc}$  and  $\omega_{zc}$  are angular velocities of the mass center of the cylinder in the body fixed frame.  $\dot{x}_c, \dot{y}_c$  and  $\dot{z}_c$  are velocities of the mass center in the body fixed frame,  $\ddot{x}_c, \ddot{y}_c$  and  $\ddot{z}_c$  are accelerations of the mass center in the body fixed frame. Similarly, Euler equations for rotary motion of the cylinder can be given as,

$$M_{xc} = I_{xc} \dot{\omega}_{xc} - (I_{yc} - I_{zc}) \omega_{yc} \omega_{zc} \quad (18)$$

$$M_{yc} = I_{yc} \dot{\omega}_{yc} - (I_{zc} - I_{xc}) \omega_{zc} \omega_{xc} \quad (19)$$

$$M_{zc} = I_{zc} \dot{\omega}_{zc} - (I_{xc} - I_{yc}) \omega_{xc} \omega_{yc} \quad (20)$$

where  $I_{xc}, I_{yc}$  and  $I_{zc}$  are second moment of inertia about the principal axes,  $M_{xc}, M_{yc}$  and  $M_{zc}$  are components of resultant moment due to external forces and couples about the non-rotating coordinate frame whose axes are momentarily aligned with the principal axes of the body.

Above Euler equations can be represented by the double gyrator rings where the gyrators are modulated by the angular velocities in the body fixed frame. Similarly, Euler equations can be generated for the piston also and it can be represented by the double gyrator rings. Generated bond graph model of above equations are shown in Fig. 3 in which G1 to G12 are the gyrator moduli taken from above equations. The position of the fixed point in the body fixed frame is  $x_2, y_2, z_2$ . The velocity of the cylinder in the body fixed frame is

$$\dot{x}_2 = \dot{x}_c + z_2 \omega_{yc} - y_2 \omega_{zc} \quad (21)$$

$$\dot{y}_2 = \dot{y}_c + x_2 \omega_{zc} - z_2 \omega_{xc} \quad (22)$$

$$\dot{z}_2 = \dot{z}_c + y_2 \omega_{xc} - x_2 \omega_{yc} \quad (23)$$

Eqs. (21)–(23) are body fixed velocities. So, it is necessary to convert it into the inertial frame by coordinate transformation block (CTF). CTF block are generated using successive multiplication of rotation matrices as follows:

$$\begin{Bmatrix} \dot{X}_2 \\ \dot{Y}_2 \\ \dot{Z}_2 \end{Bmatrix} = T_{\theta c, \psi c, \psi c} \begin{Bmatrix} \dot{x}_2 \\ \dot{y}_2 \\ \dot{z}_2 \end{Bmatrix} \quad (24)$$

where,

$$T_{\theta c, \psi c, \psi c} = \begin{bmatrix} c\theta_c & -s\theta_c & 0 \\ s\theta_c & c\theta_c & 0 \\ 0 & 0 & 1 \end{bmatrix} \begin{bmatrix} c\theta_c & 0 & s\theta_c \\ 0 & 1 & 0 \\ -s\theta_c & 0 & c\theta_c \end{bmatrix} \begin{bmatrix} 1 & 0 & 0 \\ 0 & c\psi_c & -s\psi_c \\ 0 & s\psi_c & c\psi_c \end{bmatrix} \quad (25)$$

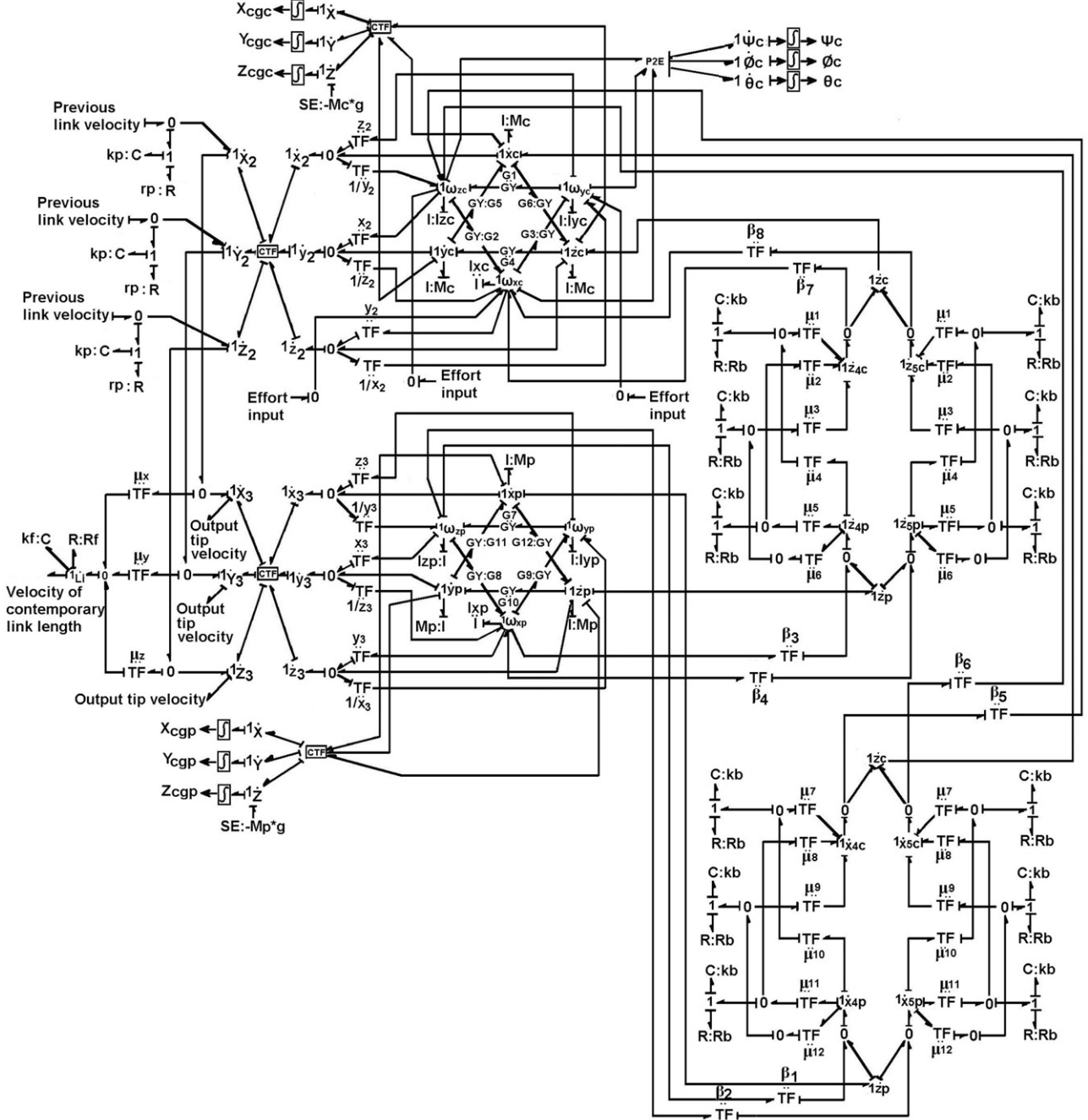


Fig. 3. Bond graph model of prismatic link.

$c\theta_c$  is shorthand for  $\cos \theta_c$ ,  $s\theta_c$  for  $\sin \theta_c$  and so on and  $\emptyset_c$ ,  $\theta_c$  and  $\psi_c$  are the Z-Y-X Cardan angles. Components of  $T_{\emptyset_c, \theta_c, \psi_c}$  are used to construct CTF block. Similarly, the velocity of the piston in the body fixed frame can be written and it can be converted into an inertial frame. It is to be noted that the required angle for CTF block are derived from the inverse transformation from body-fixed angular velocities to Euler angle rates [30].

The normal fixed velocities at the contact point 4 and 5 on the cylinder and piston along  $x$  and  $z$  directions by assuming a thin but long piston can be given as [35]

$$\dot{x}_{4c} = \dot{x}_c + \left( l - l_p - l_{cg} - \frac{d}{2} \right) \omega_{zc} \quad (26)$$

$$\dot{z}_{4c} = \dot{z}_c + \left( l - l_p - l_{cg} - \frac{d}{2} \right) \omega_{xc} \quad (27)$$

$$\dot{x}_{4p} = \dot{x}_p - \left( l_p - l_{pg} + \frac{d}{2} \right) \omega_{zp} \quad (28)$$

$$\dot{z}_{4p} = \dot{z}_p - \left( l_p - l_{pg} + \frac{d}{2} \right) \omega_{xp} \quad (29)$$

$$\dot{x}_{5c} = \dot{x}_c + \left( l - l_p - l_{cg} + \frac{d}{2} \right) \omega_{zc} \quad (30)$$

$$\dot{z}_{5c} = \dot{z}_c + \left( l - l_p - l_{cg} + \frac{d}{2} \right) \omega_{xc} \quad (31)$$

$$\dot{x}_{5p} = \dot{x}_p - \left( l_p - l_{pg} - \frac{d}{2} \right) \omega_{zp} \quad (32)$$

$$\dot{z}_{5p} = \dot{z}_p - \left( l_p - l_{pg} - \frac{d}{2} \right) \omega_{xp} \quad (33)$$

**Table 1**

Joint position for trot gait.

| Joint position corresponding to time interval | Leg 1   |         | Leg 2   |         | Leg 3   |         | Leg 4   |         |
|---|---------|---------|---------|---------|---------|---------|---------|---------|
|   | Joint 1 | Joint 2 |
| Initial joint angle                           | -1.871  | 0.622   | -1.671  | 0.537   | -1.271  | -0.622  | -1.471  | -0.537  |
| $T_o \leq t < T_1/2$                          | -1.962  | 0.944   | -1.781  | 0.602   | -1.361  | -0.602  | -1.179  | -0.944  |
| $T_1/2 \leq t < T_1$                          | -1.671  | 0.537   | -1.871  | 0.622   | -1.471  | -0.537  | -1.271  | -0.622  |
| $T_1 \leq t < T_2/2$                          | -1.781  | 0.602   | -1.962  | 0.944   | -1.179  | -0.944  | -1.361  | -0.602  |
| $T_2/2 \leq t < T_2$                          | -1.871  | 0.622   | -1.671  | 0.537   | -1.271  | -0.622  | -1.471  | -0.537  |

where  $\vec{\omega}$  indicates the body fixed angular velocity about the axis indicated in subscript. Subscript  $c$  has been used for cylinder while  $p$  has been used for the piston. The rate of change of contemporary length between two end points of prismatic link can be expressed as

$$\dot{l}_c = \mu_x (\dot{X}'_2 - \dot{X}'_3) + \mu_y (\dot{Y}'_2 - \dot{Y}'_3) + \mu_z (\dot{Z}'_2 - \dot{Z}'_3) \quad (34)$$

where  $X'_2, Y'_2, Z'_2$  and  $X'_3, Y'_3, Z'_3$  are coordinates of cylinder end and piston end respectively and  $\mu_x = \left( \frac{X'_2 - X'_3}{l_c} \right)$ ,  $\mu_y = \left( \frac{Y'_2 - Y'_3}{l_c} \right)$

and  $\mu_z = \left( \frac{Z'_2 - Z'_3}{l_c} \right)$  are moduli used to derive the relative sliding velocity between piston and cylinder at '0' junction as shown in Fig. 3. Compliance in the link is modeled by 'C' and 'R' element. For contact point mechanics, to compute contact point velocities in body fixed frame moduli  $\beta_1$  to  $\beta_4$  and  $\beta_5$  to  $\beta_8$  are determined from kinematic analysis of the cylinder and piston, respectively. Through a set of transformer moduli  $\mu_1$  to  $\mu_{12}$  similar to an expanded form of CTF block, body fixed velocities are transformed into inertial velocities and then they are implicitly constrained. The relative normal velocity between the contact point on the cylinder and the normal velocity at the contact point on the piston are implicitly constrained by contact stiffness and damping parameters,  $k_b$  and  $R_b$  respectively. The three external effort inputs are from the motor. Since the motor applies torque about body-fixed  $x$ -axis on the cylinder, two of these effort inputs are zero.

#### 2.4. Dynamics of combined body and leg links

The bond graph model is developed using above discussed body and leg dynamics. A compact and a simple presentation of a bond graph model can be carried out in multi bond graph form. Here also developed three dimensional model of quadruped robot is presented in multi bond graph form as shown in Fig. 4. TVP sub-model is shown in the 'Body' part of the multi bond graph. It takes the angular velocity from a body  ${}^B(\vec{\omega}_B)$  (obtained from EJS) and translational velocity  ${}^A(\vec{V}_B)$  (decided by body mass) as input and gives out the velocity of {0} frame to the link 1 of each leg. Frames {0} and {1} are coincident for each leg. Hence, the velocity of frame {1} is same as the frame {0}. 'Leg' sub model in the multi bond graph represents a two DOF leg. It takes the angular and linear velocity of body and joint torques about  $x$ -axis as input. It uses AVP and TVP sub-models of links 1 and 2 and gives out leg tip velocity as output. This sub-model furnishes complete dynamics of a two link leg. The various sub-models shown in Fig. 4 for leg 1 can also be used to model legs 2, 3 and 4. The leg tip sub-model in Fig. 4 represents the modeling of leg tip-ground interaction. An 'R' element is appended to '1' junction of each leg in the  $X$  and  $Y$  direction, to model the frictional resistance offered by ground. Similarly, 'C' and 'R' elements are attached in  $Z$  direction to model the normal reaction force from the ground. Leg tip position sensors in each direction yields the leg tip position coordinates. A systematic construction of bond graph model yields a dynamics expression that can be written in matrix form as

$$\vec{\tau}_i = [A(\theta) \ddot{\theta} + B(\theta, \dot{\theta}) + C(\theta)]_i - J_i^T \vec{F}_i \quad (35)$$

where  $\vec{\tau}$  is the  $2 \times 1$  matrix of joint torque and  $\vec{F}$  is the  $3 \times 1$  vector

of the ground contact force of leg  $i$ ,  $J$  is the Jacobian matrix,  $A(\theta)$  is the  $3 \times 3$  mass matrix,  $B$  is a  $3 \times 1$  matrix of centrifugal and Coriolis terms and  $C(\theta)$  is a  $3 \times 1$  matrix of gravity terms. A pad is used to avoid differential causality. Pads are artificial compliances/lumped flexibilities that can be used in bond graph [36,37]. Bond graph model of above discussed body and leg dynamics is developed in SYMBOLS software [38].

Compliance in the link improves locomotion of quadruped robot. But over compliance reduces locomotion speed and also affect posture disturbance. So, most suitable value of compliance is must for specific robot configuration. This objective can be achieved by simulating bond graph model of quadruped. Number of simulations can be carried out by varying the compliance (which is discussed in coming section), and its values can be finalized for maximum locomotion speed of robot. This stiffness and load coming on each leg becomes the key parameters for designing the spring used in prismatic link. Number of turns of spring ' $n$ ' can be decided as

$$n = \frac{\delta G d}{8 W C^3} \quad (36)$$

where  $W$  is load,  $\delta$  is axial deflection derived from load ( $W$ )/stiffness ( $K$ ),  $C$  is spring index derived from coil diameter ( $D$ )/wire diameter ( $d$ ), and  $G$  is the Modulus of rigidity of the spring material. Here,  $W$  is the dynamic load estimated from simulations and the spring design is valid only when the inertial effects of the spring are neglected, i.e., when the rigid-body acceleration is not very large.

#### 2.5. Joint rotation for locomotion

Walk can be classified as "static walk" and "dynamic walk". In static walk stability is maintained by keeping, at least three feet planted on the ground and maintaining the center of gravity within the support polygon. In dynamic walk stability is maintained by continuously moving either the feet or the body to maintain balance. Alexander [39] shows various gait patterns followed by four legged animals. Here statically stable gait 'Amble' and dynamically stable gait 'Trot' are considered for validation of dynamic model. In case of trot gait one pair of diagonal legs moves forward while other pair remains on the ground, which reverses in next phase of locomotion. In case of statically stable amble gait, at a time only one leg moves forward while remaining legs maintain contact with the ground. Here, legs are operated one by one in 1-4-2-3 sequence. Both the gaits are shown in Fig. 5, where dark line indicates corresponding leg contact with the ground. Now, to simulate the bond graph model in any of the gait, it is necessary to know rotation required at each joint so that a required voltage can be supplied to get the desired rotation of a joint. Thus, to determine a joint rotation, for leg forward and body forward movement, graphical analysis is carried out. Graphical analysis as shown in Fig. 6 gives an idea about a joint rotation required for the said movement. From this, joint position with reference to time is listed in Table 1 for trot gait. Here, cubic curve is fitted for smooth joint rotation. The required voltage for the said movement is supplied by actuator which is controlled by Proportional–Integral–Derivative (PID) controller and can be represented as,

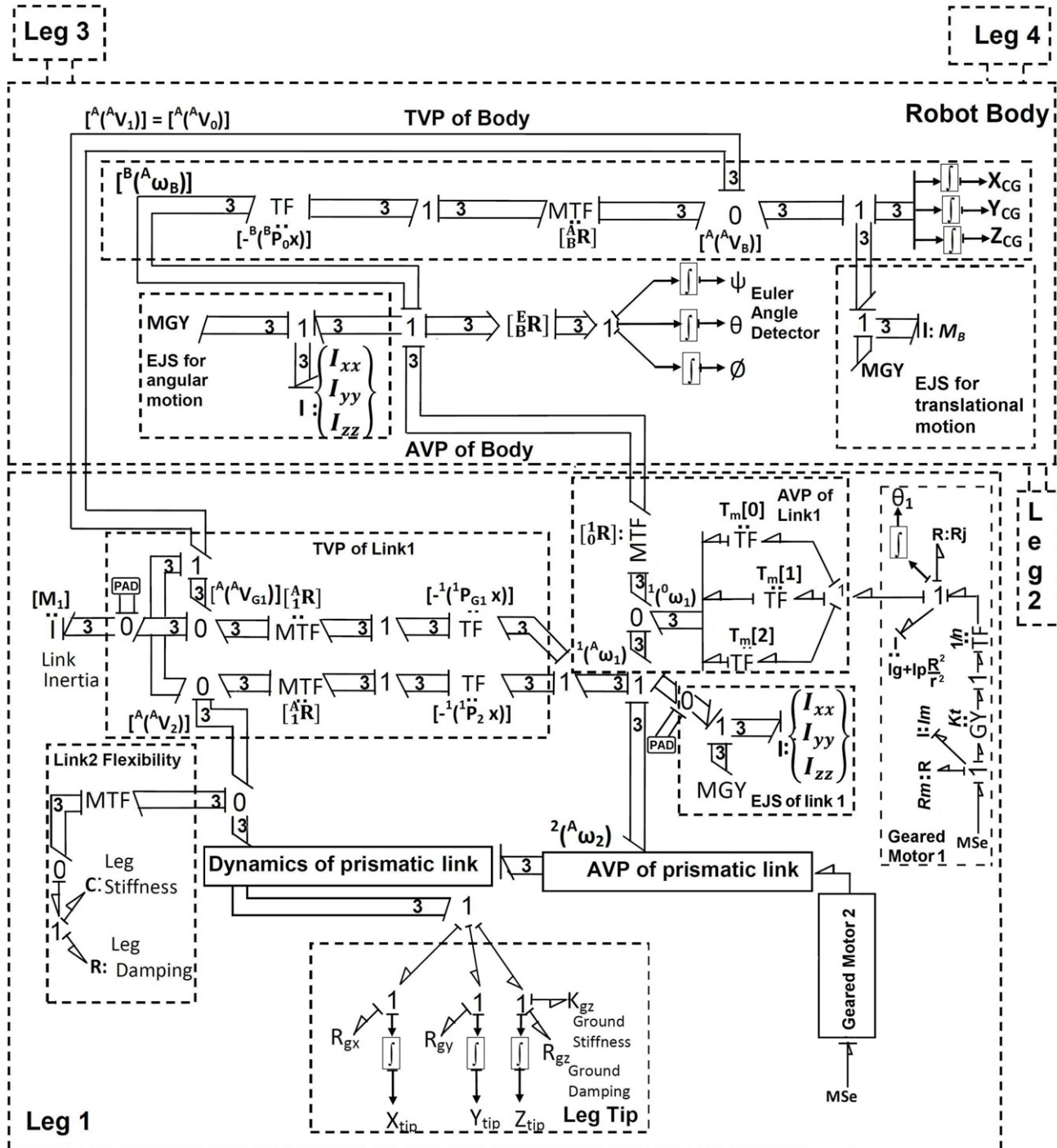


Fig. 4. Multi bond graph of a quadruped robot.

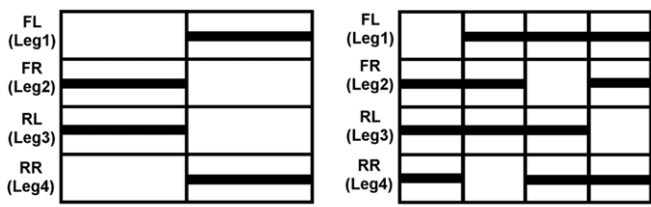


Fig. 5. Trot and amble gait.

$$V = K_P (\theta_d - \theta_a) + K_D (\dot{\theta}_d - \dot{\theta}_a) + K_I \int (\theta_d - \theta_a) dt \quad (37)$$

where  $V$  is the input voltage supplied to the joint actuator of leg;  $K_P$ ,  $K_D$  and  $K_I$  are the proportional, derivative and integral gains, respectively;  $\theta_d$  is the desired position,  $\theta_a$  is the actual measured angular position,  $\dot{\theta}_d$  is the desired joint velocity, and  $\dot{\theta}_a$  is the actual measured joint velocity.

### 3. Results and discussions

Above discussed bond graph model can be used for various research aspects pertaining to quadruped robot. In this section first trot gait is simulated using joint rotation discussed in Section 2.5 and its results are verified through animation and experimental results. In trot gait, diagonally opposite pairs of legs are actuated

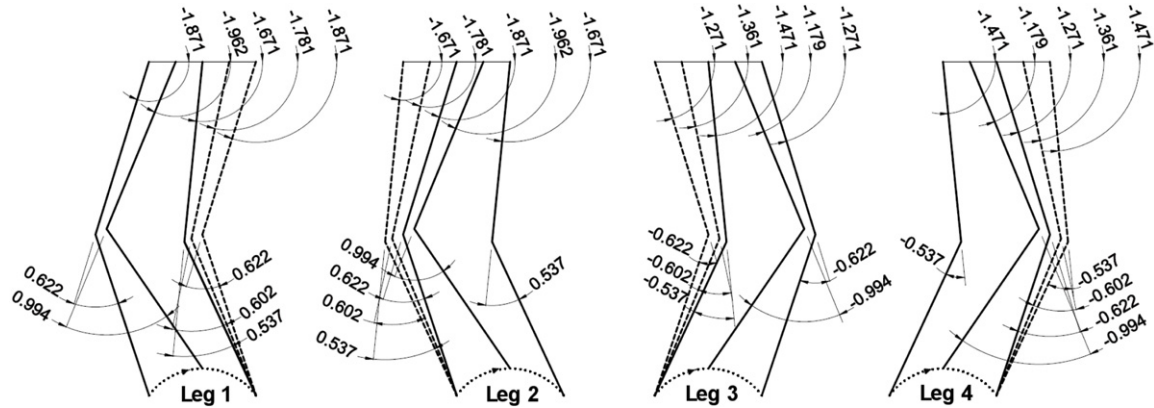


**Fig. 6.** Graphical representation of leg and body movement.

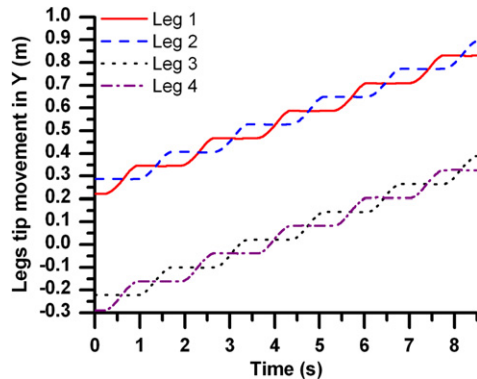


**Fig. 7.** Legs tip movement in Y direction.

together to move forward. This is inspired from the way a horse moves. This two-beat diagonal gait minimizes the shift in body centroid and ensures good dynamic stability. Therefore, the quadruped can achieve higher locomotion speed with this gait. The usefulness of a dynamic model comes when dynamic forces are significant. Therefore, trot gait has been considered in this article for model validation. In addition, the amble gait is demonstrated in this section with turning motion. Influence of compliance is studied on locomotion parameter. The performance measure is evaluated based on energy efficiency.

### 3.1. Simulation, animation and experiment results of locomotion with trot gait

#### 3.1.1. Simulation results for locomotion with trot gait

Bond graph model is simulated for trot gait for which controlled efforts are supplied to the actuator to reach to required joint position shown in Table 1. Input parameter considered for the simulation is listed in Table B.1 of Appendix B. Positive Y direction is considered as forward direction. Time duration for each cycle is 1.7 s. Simulation is carried out for five cycles. Fig. 7 shows leg tip displacement in Y direction, while Fig. 8 shows leg tip displacement in Z direction. Fig. 9 shows body CG movement in X, Y and Z directions. It shows robot moves in a forward Y direction. Legs joint rotations for the said motion are shown in Fig. 10(a) and 10(b) for joints 1 and 2 respectively. Similar way, simulation can be carried out for other gait also.

#### 3.1.2. Animation results for locomotion with trot gait

Animation of above discussed locomotion strategy of quadruped robot is carried out in SYMBOLS Shakti Animator [38]. The physical characteristics of certain selected aspects of bond graph model

can be directly visualized in this animator, for a better understanding of intrinsic behavior quadruped robot. Animation of quadruped robot is created from the simulation results. Fig. 11 shows animation frames of quadruped robot walking. To maintain neatness of the figure only two frames of animations are shown. First frame indicates starting position and second frame indicates final position of quadruped robot at the end of five cycles. Path traced by tip of leg 1 is also shown in this figure.

#### 3.1.3. Experiment result for locomotion with trot gait

Above presented simulation and animation results show that quadruped robot travels 0.61 m in five cycles with help of the developed locomotion strategy. The same strategy is implemented in the physical model. As shown in Fig. 1(a), the physical model of quadruped robot contains total eight number of Maxon brushless DC motors. To control these motors, eight Maxon (EPOS) controllers are used. One of those acts as master and the remaining seven act as slave controllers. This robot has approximately 15 kg weight and its body length and width are 0.5 m and 0.42 m, respectively. Its height is 0.479 m. Above discussed locomotion strategy is applied on physical model and it is observed that it travels 0.55 m in five cycles. Fig. 12 shows few snaps taken during locomotion of quadruped robot. Fig. 12(a) shows beginning of a cycle, Figs. 12(b) and (c) show leg motion in intermediate stages and Fig. 12(d) shows end of a cycle. For the movements detailed above, the joint rotations performed by all legs are shown in Fig. 13.

The pattern of joint rotations during the experiments is almost the same as simulation. There are always some assumptions made for numerical modeling of any system. Here, the assumptions for quadruped modeling are: mass center of link is located at the mid of its length, center of gravity of top body is located at the center of body, top body and upper links are rigid, joint rotation allows rotation of link about one axis only, robot is walking on hard surface and on even terrain, and external force and moment effects are negligible. Condition of the surface, on which physical robot walks, affects robot locomotion. It seems from our simulation, animation and experimental results that little deviations observed in experiments are because of the assumptions considered during modeling and uncertain surface conditions like its roughness, friction and elevation. These experimental results support the correctness of the dynamic model generated in bond graph.

### 3.2. Simulation of turning motion

It is understood that if robot leg has more than one degree of freedom with joint rotation about different axis then only other than straight line motion is possible. The discussed robot configuration has two DOF per leg but both axes of rotation are same, i.e., about X. Thus each leg tip travels same distance while in

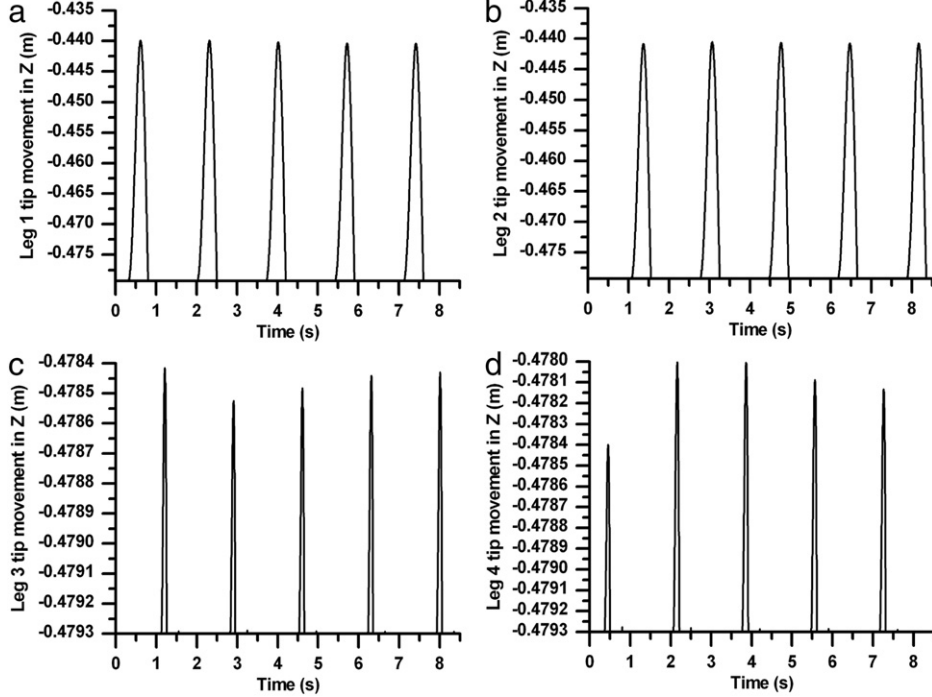


**Fig. 8.** Legs tip Z displacement; (a) Leg 1, (b) Leg 2, (c) Leg 3, (d) Leg 4.

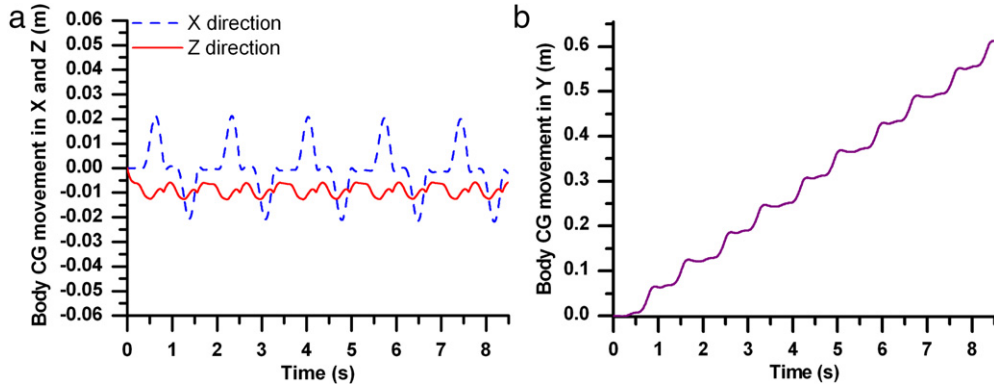


**Fig. 9.** Body CG movement; (a) X and Z direction, (b) Y direction.

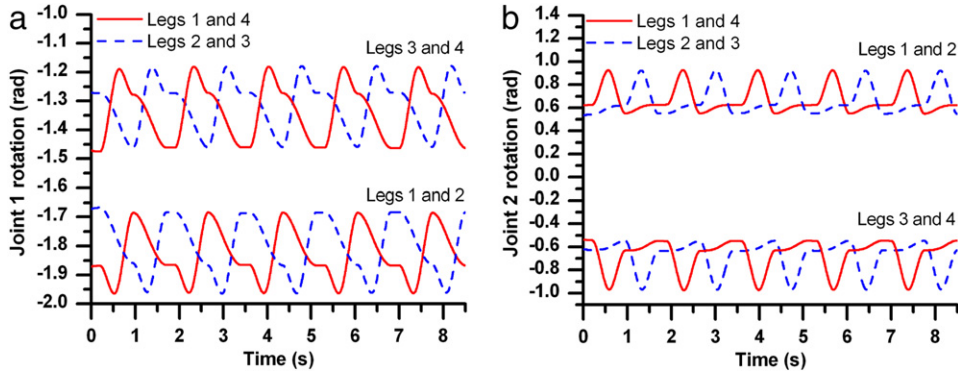


**Fig. 10.** Joints rotation: (a) Joint 1 and (b) Joint 2.

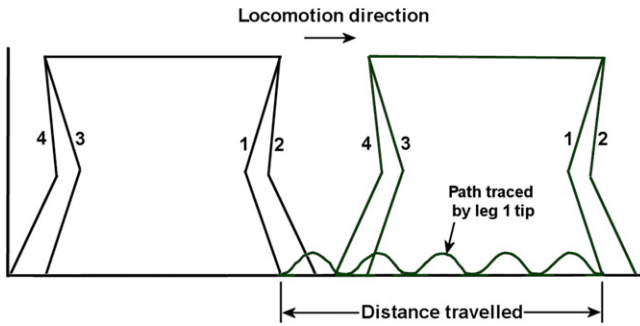
motion during one cycle and robot has straight line motion. If one side of both the leg tips travels same distance but different from opposite side of leg tips (i.e., leg 1 and 3 tip travels same distance but they are different from leg 2 and 4 tip travels), then this motion gives a turn instead of moving in straight line. This concept has been demonstrated using amble gait. Simulation and animation are

carried out for twenty cycles. Each cycle takes 0.9 s. Fig. 14 shows animation frames of quadruped locomotion which moves straight for initial five cycles (A) then it takes turn for next ten cycles (B) and finally moves straight for remaining five cycles (C). In this figure path traced by hip joints and body CG are shown. Joint position corresponding to time interval is shown in Table 2.

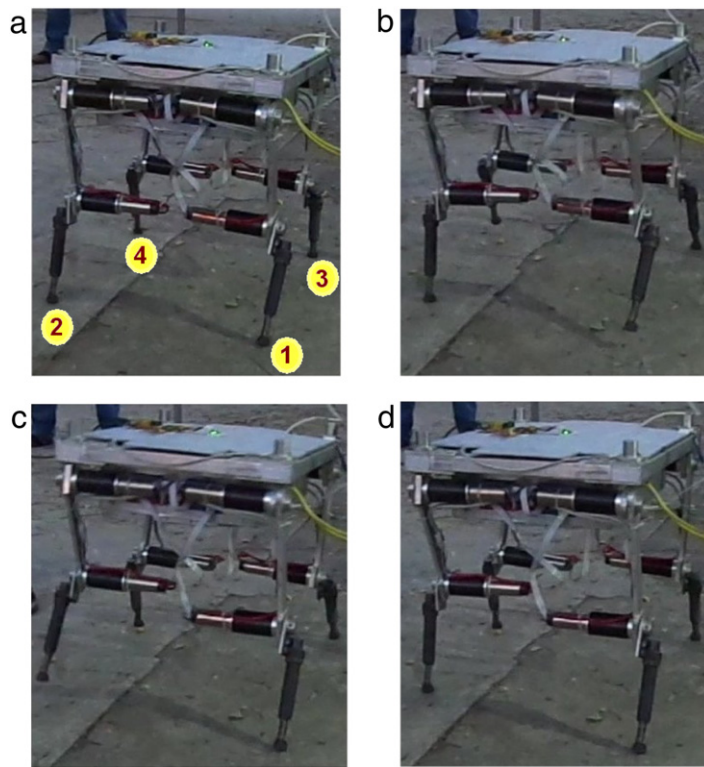
**Table 2**

Joint position of amble gait for turning motion.

| Joint position corresponding to time interval | Leg 1   |         | Leg 2   |         | Leg 3   |         | Leg 4   |         |
|---|---------|---------|---------|---------|---------|---------|---------|---------|
|   | Joint 1 | Joint 2 |
| Initial joint angle                           | -1.871  | 0.622   | -1.747  | 0.586   | -1.271  | -0.622  | -1.395  | -0.586  |
| $T_0 \leq t < T_1/2$                          | -1.979  | 1.199   | -1.781  | 0.602   | -1.323  | -0.615  | -1.431  | -0.564  |
| $T_1/2 \leq t < T_1$                          | -1.417  | 0.265   | -1.813  | 0.613   | -1.381  | -0.593  | -1.471  | -0.537  |
| $T_1 \leq t < T_2/2$                          | -1.530  | 0.407   | -1.843  | 0.620   | -1.448  | -0.554  | -1.179  | -0.994  |
| $T_2/2 \leq t < T_2$                          | -1.618  | 0.494   | -1.871  | 0.622   | -1.523  | -0.494  | -1.271  | -0.622  |
| $T_2 \leq t < T_3/2$                          | -1.694  | 0.554   | -1.962  | 0.944   | -1.611  | -0.407  | -1.299  | -0.620  |
| $T_3/2 \leq t < T_3$                          | -1.760  | 0.593   | -1.671  | 0.537   | -1.725  | -0.265  | -1.328  | -0.613  |
| $T_3 \leq t < T_4/2$                          | -1.819  | 0.615   | -1.710  | 0.564   | -1.162  | -1.199  | -1.361  | -0.602  |
| $T_4/2 \leq t < T_5$                          | -1.871  | 0.622   | -1.747  | 0.586   | -1.271  | -0.622  | -1.395  | -0.586  |

**Fig. 11.** Animation frames of quadruped robot locomotion with trot gait.

**Fig. 15** shows body CG X motion while **Figs. 16** and **17** show body CG Y and Z motions, respectively. Leg tip motion in X and Y directions are shown in **Figs. 18** and **19**, respectively. As discussed above, it is necessary to have different joint rotations for this kind of locomotion. Joints 1 and 2 rotations carried out of all legs for the said motions are shown in **Figs. 20** and **21**, respectively. Thus, by having combination of different joint angles, motion other than straight line is possible.

**Fig. 12.** Experiment on physical model. (a) Initial position, (b) and (c) Intermediate positions, (d) End of cycle.

### 3.3. Influence of compliance on locomotion parameter

Compliance affects locomotion speed and posture disturbance. In this section, attempt is made to study influence of compliance on both these locomotion parameter. Developed bond graph model is simulated for various compliance and damping value of the same damping ratio. The body CG travels (indicating motion of robot in forward direction) and posture disturbance are analyzed. **Fig. 22(a)** shows body CG travels by quadruped robot and **Fig. 22(b)** shows range posture disturbance in roll and pitch during the locomotion.

It is concluded from the results that as the stiffness decreases, the body CG travel reduces. Body CG travel does not increase noticeably after increasing the stiffness further than about 7000 N/m.

It is also seen from the results that the posture disturbance range at roll and pitch becomes higher at higher stiffness. It is always desirable to have minimum posture disturbance with maximum body CG travel. Thus, for our robot configuration we have chosen 5000 N/m stiffness as a trade-off, which gives good locomotion with relatively low range of posture disturbances in roll and pitch.

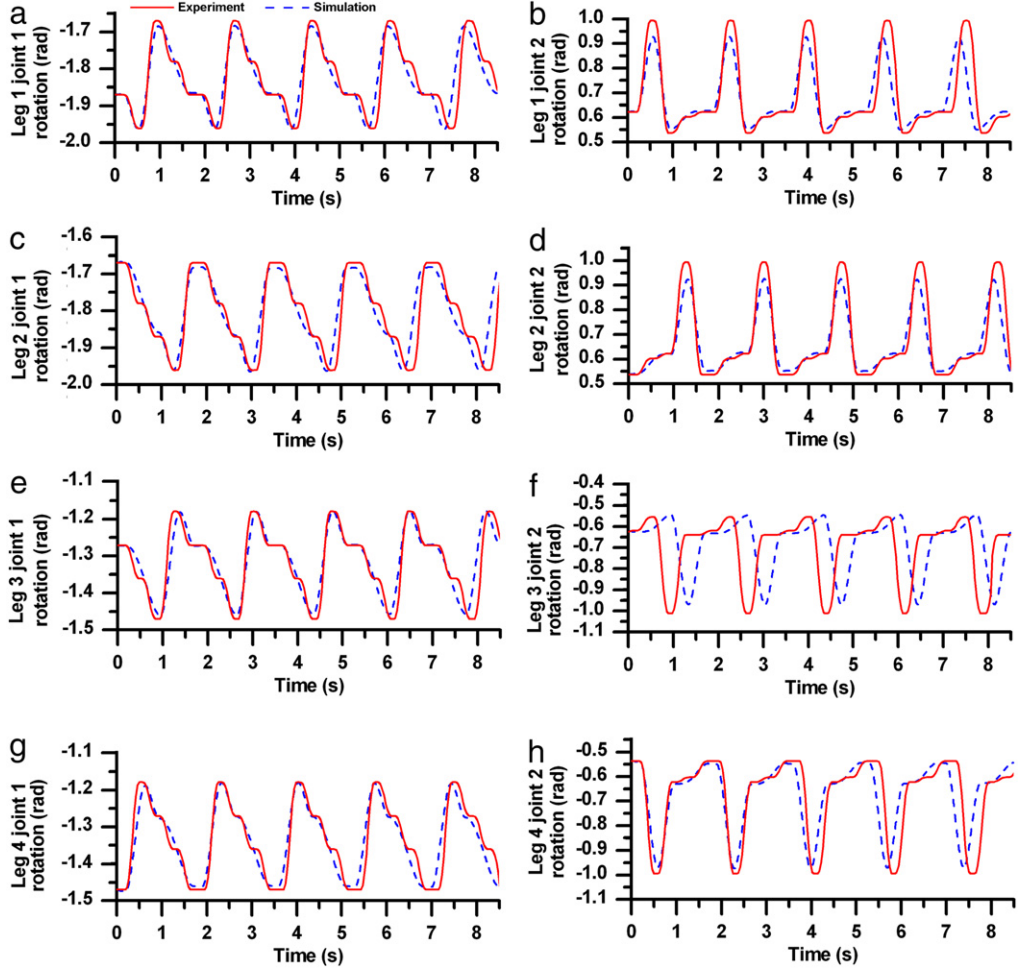


**Fig. 13.** Joints rotations during experiment and simulation. (a) Leg 1 joint 1, (b) Leg 1 joint 2, (c) Leg 2 joint 1, (d) Leg 2 joint 2, (e) Leg 3 joint 1, (f) Leg 3 joint 2, (g) Leg 4 joint 1, (h) Leg 4 joint 2.

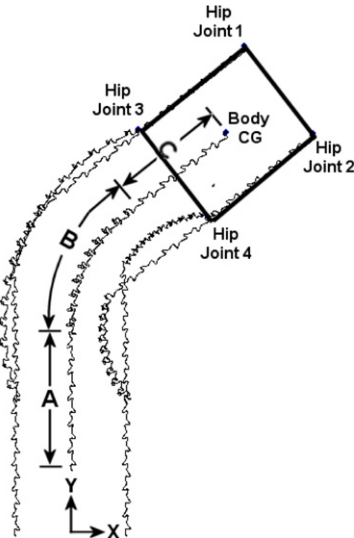


**Fig. 14.** Animation frames in top view of quadruped robot in turning motion.

#### 3.4. Performance measures through energy efficiency

Robot walk may be evaluated by stability, maximum speed and energy consumption. Parameters like a type of gait, stride length, duty factor, length of leg, joint angle and rotation are deciding the above-mentioned performance criteria. To discuss advantage

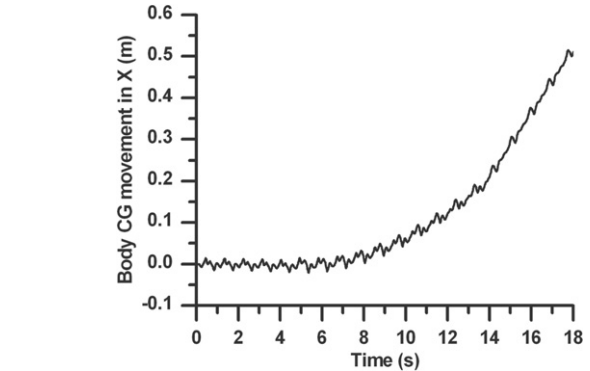


**Fig. 15.** Body CG movement in X direction.

and disadvantage of different designs and control strategies, it is necessary to evaluate and compare robot performance and abilities with respect to common criteria. A common measure to evaluate and compare the energy efficiency of vehicles is the energy consumption per unit distance. To justify the comparison, mass moved and velocity obtained should also be considered with the cost of locomotion. We are comparing here quadruped walk with specific resistance ( $\epsilon$ ). The specific resistance [40,41] is a dimensionless number describing the energy efficiency of a mobile system. The specific resistance is defined as

$$\epsilon = \frac{P(v)}{mgv} = \frac{E}{mgd} \quad (38)$$

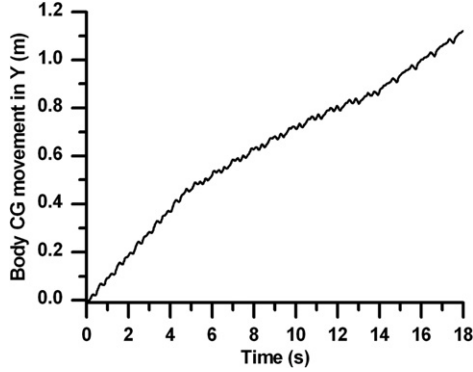


Fig. 16. Body CG movement in Y direction.

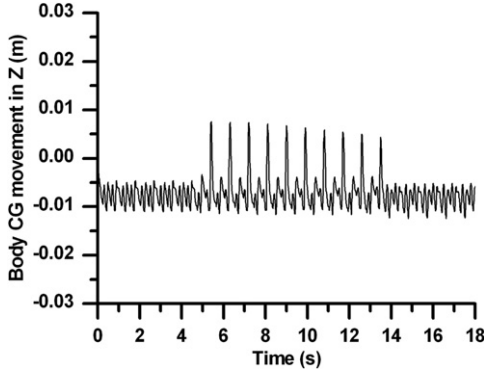


Fig. 17. Body CG movement in Z direction.

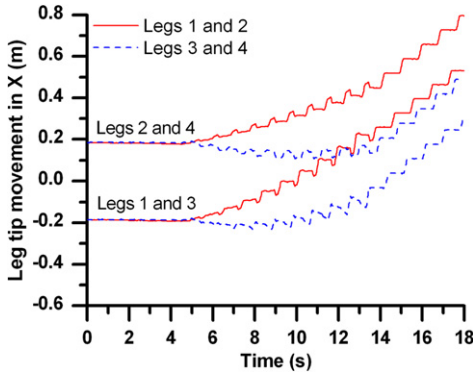


Fig. 18. Leg tip movement in X direction.

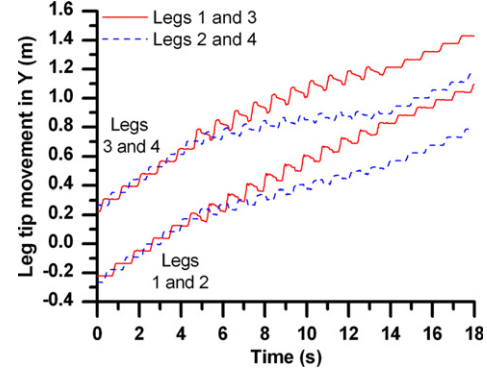


Fig. 19. Leg tip movement in Y direction.

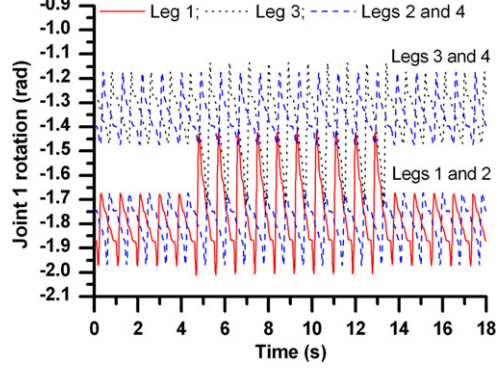


Fig. 20. Joint 1 rotation of legs.

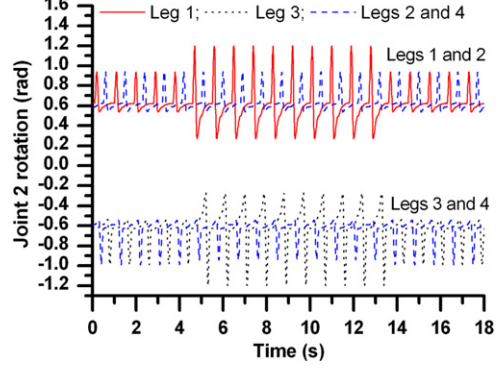


Fig. 21. Joint 2 rotation of legs.

where  $P(v)$  is the power needed to move the body with velocity  $v$ ,  $m$  is the mass of the system,  $g$  is the acceleration due to gravity,  $d$  is the distance traveled and  $E$  is the energy spent. Since velocity is not constant in a cycle, energy spent to move unit weight by unit distance is preferred as the performance measure. Sufficient number of cycles of motion till steady-state is reached should be considered for evaluation of specific resistance. Lower specific resistance implies higher energy efficiency.

#### 3.4.1. Energy efficient structure of quadruped robot

In this section, energy efficiency of rigid legged and compliant legged robots are evaluated and compared. Locomotion gait is considered as trot for both the cases. The above developed bond graph model for compliant legged robot was modified to generate the model of rigid legged robot. This is done by locking the sliding motion of the piston within the prismatic link; thereby retaining the same mass parameters in both the models. The locking is performed through a high-stiffness virtual spring which is called

a pad in bond graph terminology. Both rigid legged and compliant legged models are simulated for same speed which is fixed at 0.42 m distance traveled in 4.5 s, i.e. with an average locomotion speed of 0.093 m/s. The same speed requirement is satisfied by manually tuning the controller parameters and the cycle time durations. Fig. 23(a) shows body CG travels by rigid legged quadruped robot in trot gait. Fig. 23(b) shows body CG travels by compliant legged robot in trot gait. Sensors are placed at the actuators in bond graph models to extract the power consumption data. The specific resistance defined in Eq. (38) is evaluated for both these cases considering robot mass as 15 kg and gravitational acceleration as  $9.81 \text{ m/s}^2$ . It was found that the specific resistance for the compliance legged model is 0.925 while it is 1.10 for rigid legged model. It is known that smaller the specific resistance, higher the energy efficiency [40–42]. So from the above results, smaller specific resistance of compliant legged robot implies that it is energy efficient than rigid legged robot. Leg compliance reduces impact induced bounce and allows for better grip; thereby improving the locomotion efficiency. However, it may be noted that too low or too high

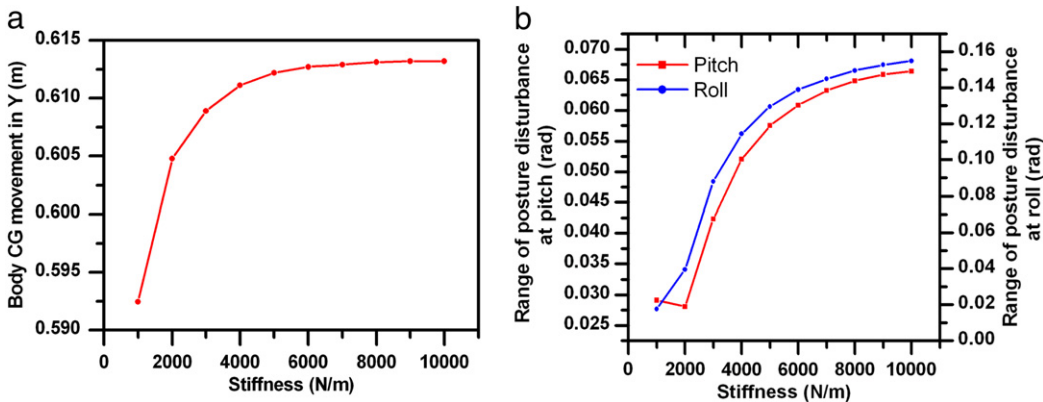


**Fig. 22.** Influence of compliance on (a) body CG travels, and (b) posture disturbance.

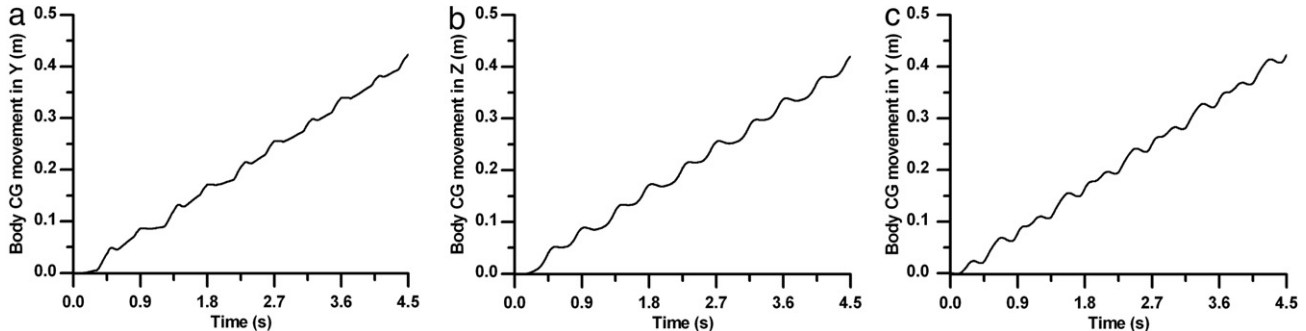


**Fig. 23.** Body CG Y displacement in various conditions. (a) Rigid legged model with trot gait, (b) Compliant legged model with trot gait, (c) Compliant legged model with amble gait.

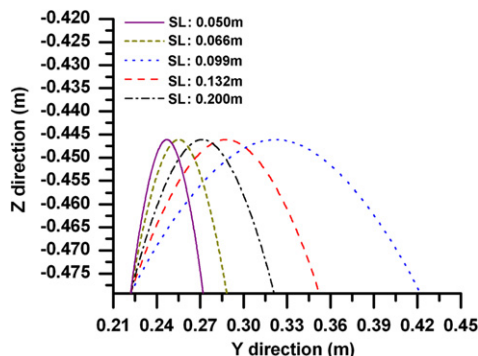


**Fig. 24.** Leg tip motion in YZ plane for different step length with same leg lift.

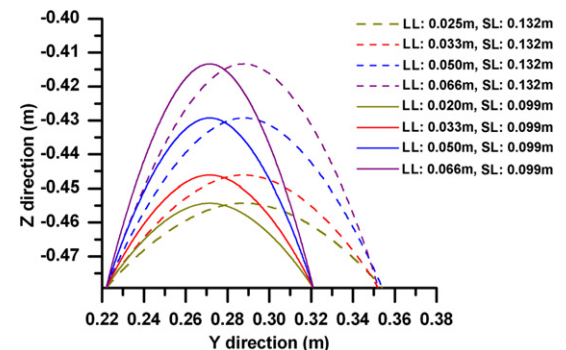


**Fig. 26.** Leg tip motion in YZ plane for different foot height with same step length.

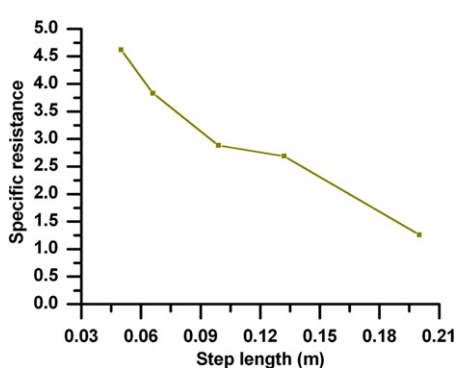


**Fig. 25.** Specific resistance for different step length with same leg lift.

stiffness reduce grip and increase losses due to sliding between the piston and cylinder of the prismatic pairs. Thus, there is an optimum value of compliance where lowest specific resistance is

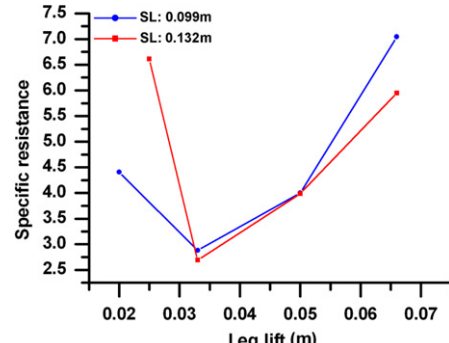


**Fig. 27.** Specific resistance for different leg lift with same step length.

possible. That optimum value has not been obtained here. We have merely compared the performance of the compliant legged robot with design parameters chosen from Fig. 22 with a rigid legged robot.

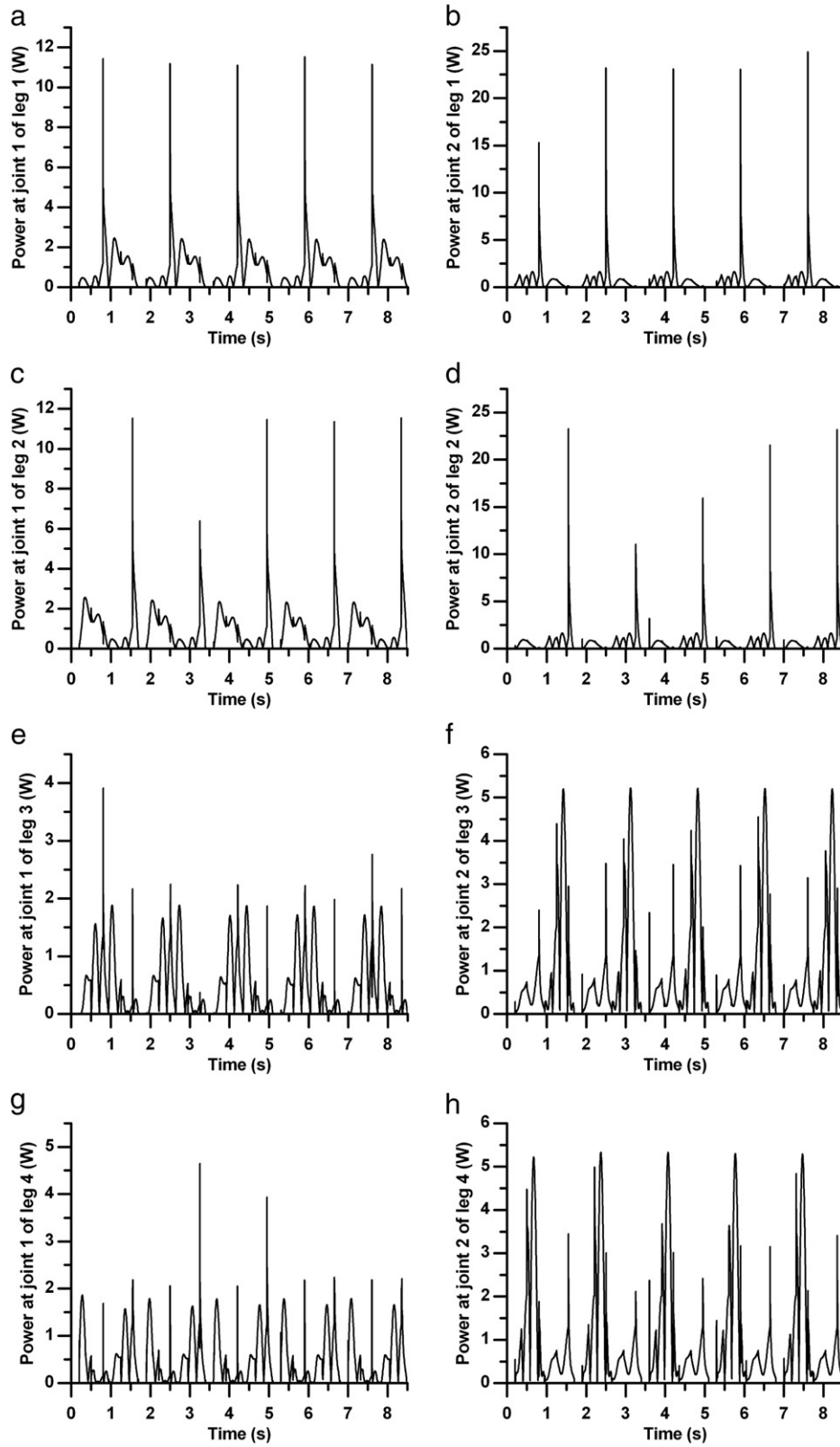


**Fig. 28.** Power at each joint of leg during walk with trot gait (a) Leg 1 joint 1, (b) Leg 1 joint 2, (c) Leg 2 joint 1, (d) Leg 2 joint 2, (e) Leg 3 joint 1, (f) Leg 3 joint 2, (g) Leg 4 joint 1, (h) Leg 4 joint 2.

#### 3.4.2. Energy efficient locomotion gait

In this section, energy efficient locomotion gait is evaluated from the static and dynamic gaits. The trot gait is considered as a dynamically stable gait, while the amble gait is considered as a statically stable gait. Specific resistance of trot gait of compliant legged

structure is just evaluated in Section 3.4.1. Thus, it is only need to evaluate specific resistance of quadruped walking with amble gait for comparison. Model is simulated for amble gait. Here also results are compared for the same speed which is obtained by tuning controller parameters and cycle duty times. Body CG displacement

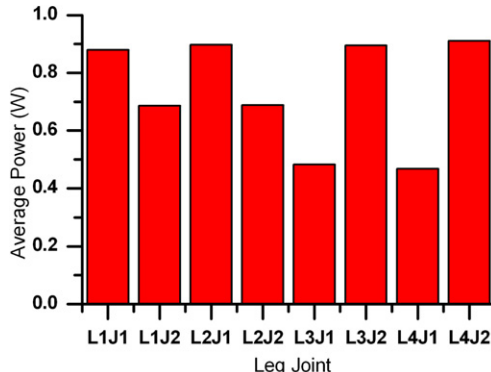


Fig. 29. Mean power at each actuator.

obtained in Y direction (along the longitudinal axis) for amble gait is shown in Fig. 23(c). Results obtained are used to evaluate Eq. (38) which gives the specific resistance of the amble gait as 6.71. From this result it seems that specific resistance of the trot gait is smaller. Thus the trot gait is energy efficient than the amble gait.

### 3.4.3. Energy efficient foot trajectory

Foot trajectory in case of walking robot has two main parameters; leg lift (LL) and step length (SL), which almost decides the foot trajectory of leg tip. However, the way leg tip reach to LL decides exact curve. Here, numbers of simulations are carried out to analyze the effect of LL and SL. For this analysis dynamic model should be controlled in workspace mode. Assumptions considered for the analysis are: robot walks in straight line and on even terrain with trot gait.

First, simulations are carried out for different SL by keeping LL fixed as 0.033 m. Fig. 24 shows given leg tip motion in Y and Z directions. Specific resistance for this run are plotted in Fig. 25 which indicates that for fixed LL as SL increases the specific energy decreases thus walk becomes more and more energy efficient.

Next, simulations are carried out for different LL by keeping SL fixed. Here, two sets of simulations are performed for SL as 0.099 and 0.132 m. Fig. 26 shows given leg tip trajectory while Fig. 27 shows specific resistance. In both the cases it is observed that as LL increases specific resistance increases thus walk becomes less energy efficient. At the same time too much low LL also reports less energy efficient as its specific resistance goes high.

Thus from all these analyses it can be concluded that for energy efficient walk, SL should be as high as possible and LL should be low if it walks on even terrain. For 0.033 m LL, 0.200 m SL gives most energy efficient walks as its specific resistance is lowest. However, for different size of robot best combination will be differing.

### 3.4.4. Power consumption

Developed bond graph model can be useful for the actuator sizing such as determining the actuator efforts, power rating and slew rates. Bond graph modeling technique allows complete analysis in this regard [30,43,44]. Fig. 28 shows power at each actuator of quadruped robot walking with the trot gait. Fig. 28(a) and (b) shows power at joint 1 and joint 2 respectively of leg 1. Fig. 28(c) and (d) shows power at joints 1 and 2 respectively of leg 2. Fig. 28(e) and (f) shows power at joint 1 and joint 2 respectively of leg 3. Fig. 28(g) and (h) shows power at joints 1 and 2 respectively of leg 4.

Mean power drawn at each actuator is shown in Fig. 29 for each joint. These results are helpful in sizing the actuators for experiments.

## 4. Conclusions

A three dimensional model of compliant legged quadruped robot using bond graph has been developed. The legs contain telescopic tubes with axial compliance and the model considers its detailed dynamics. The developed model is first simulated for trot gait, and the obtained simulation and animation results are compared with the experimental results for model validation. The developed model is useful for the various research activities pertaining to quadruped control. Its versatility is demonstrated by performance analysis, which shows that the compliant legged robot is more energy efficient than rigid legged robot, a dynamically stable trot gait is more energy efficient than a statically stable amble gait, and a foot trajectory consisting of maximum possible step length with minimum leg lift gives energy efficient performance. Influence of compliance on locomotion parameters are studied and best suitable compliance value for the robot is obtained. Turning motion of the robot is demonstrated by differential leg tip velocity of robot. In future, it is envisaged to use this model for work space control, posture control, and fault accommodation of the quadruped robot.

## Acknowledgments

The work of Mehul M. Gor, Pushparaj Mani Pathak, and A.K. Samantaray has been funded by DST, India under Indo-Korea Joint Research in Science and Technology vide Grant No. INT/Korea/P-13. Mehul M. Gor is thankful to G.H. Patel College of Engineering & Technology, Gujarat, India for allowing him to carry out research work at IIT Roorkee. The work of J.-M. Yang and S.W. Kwak was supported by the National Research Foundation of Korea grant funded by the Korea government (MEST) (No. NRF-2011-0027705). Authors are thankful to B.Tech. students Divye, Kamran, Piyush, Param and Rohan for their assistantship in developing the set-up and conducting the experiments.

## Appendix A

### Nomenclature

|                             |  |
|-----------------------------|--|
| $\{A\}$                     | Inertial frame   |
| $\{B\}$                     | Robot body frame   |
| $c_i, s_i$                  | $\cos(\theta_i), \sin(\theta_i)$   |
| $d$                         | Width of a piston of a prismatic link  |
| $F$                         | Force  |
| $F_{xc}, F_{yc}, F_{zc}$    | External force acting at the cylinder body fixed x, y and z axes                 |
| $h$                         | Angular momentum   |
| $i$                         | Link number, frame number  |
| $I_{rot}$                   | Rotor inertia  |
| $I_{xb}, I_{yb}, I_{zb}$    | Moment of inertia of the robot body about x, y, and z axes                       |
| $I_{xx1}, I_{yy1}, I_{zz1}$ | Moment of inertia of the upper link of robot leg about x, y and z axes           |
| $I_{xxc}, I_{yyc}, I_{zzc}$ | Moment of inertia of the cylinder part of a prismatic link about x, y and z axes |
| $I_{xpp}, I_{ypp}, I_{zpp}$ | Moment of inertia of the piston part of a prismatic link about x, y and z axes   |
| $k_b$                       | Contact point stiffness at the piston cylinder of prismatic link                 |
| $k_f$                       | Flexibility due to hydraulic pressure inside the cylinder of prismatic link      |
| $K_{gx}, K_{gy}, K_{gz}$    | Ground contact stiffness in x, y, and z direction                                |
| $K_I$                       | Integral gain of controller  |
| $K_P$                       | Proportional gain of controller  |
| $K_D$                       | Derivative gain of controller  |

|                          |   |   |  |
|--------------------------|---|---|--|
| $l_c$                    | Contemporary length of prismatic link                                   | $R_f$                                   | Damping between piston and cylinder of prismatic link  |
| $l_{cg}$                 | Distance of cylinder CG from a cylinder end frame of prismatic link     | $R_{gx}, R_{gy}, R_{gz}$                | Ground contact resistance in $x$ , $y$ , and $z$ direction                                   |
| $l_i$                    | Length of link $i$  | $r_{ix}, r_{iy}, r_{iz}$                | Position of the frame $\{0\}$ of $i$ th leg with respect to the body CG                      |
| $l_p$                    | Length of a piston and piston rod of prismatic link                     | $R_m$                                   | Motor resistance   |
| $l_{pg}$                 | Distance of piston CG from a piston end frame of prismatic link         | $t$                                     | Time   |
| $L_m$                    | Motor inductance  | $v_x, v_y, v_z$                         | Translational velocities of the body   |
| $m_b$                    | Mass of the body  | $\theta_i$                              | Angular displacement of frame $i$  |
| $m_c$                    | Mass of cylinder part of the prismatic link                             | $\tau$                                  | Torque   |
| $m_{li}$                 | Mass of link $i$  | $\psi, \theta, \phi$                    | Euler angles representing a robot body rotation about $x, y, z$ axis of the body fixed frame |
| $m_p$                    | Mass of a piston and piston rod of a prismatic link                     | $\psi_c, \theta_c, \phi_c$              | Cardan angles about $x, y, z$ axis of the moving fixed frame                                 |
| $M_{xc}, M_{yc}, M_{zc}$ | External moment acting at the cylinder body fixed $x, y$ , and $z$ axes | $\omega$                                | Angular velocity   |
| $n$                      | Gear ratio  | $\omega_{xc}, \omega_{yc}, \omega_{zc}$ | Angular velocities of the mass center of the cylinder in the body fixed frame                |
| $p$                      | Translational momentum  |   |  |
| ${}^B R_A$               | Transformation from body frame $\{B\}$ to inertial frame $\{A\}$        |   |  |
| $R_b$                    | Contact point resistance at the piston cylinder of prismatic link       |   |  |

## Appendix B

See Table B.1.

**Table B.1**  
Input parameter.

| Parameters<br><i>Leg parameters</i>  |  | Value                       |
|--|--|-----------------------------|
| First link length of leg ( $l_1$ )   |  | 0.225 m                     |
| Mass of first link ( $M_{l1}$ )  |  | 1.11 kg                     |
| Mass of cylinder part of the prismatic link ( $M_c$ )  |  | 0.3 kg                      |
| Mass of piston part of the prismatic link ( $M_p$ )  |  | 0.2 kg                      |
| Inertia of Link 1  |  |                             |
| $I_{xx1}$  |  | 0.013346 kg m <sup>2</sup>  |
| $I_{yy1}$  |  | 0.0073965 kg m <sup>2</sup> |
| $I_{zz1}$  |  | 0.011563 kg m <sup>2</sup>  |
| Inertia of cylinder part of prismatic link   |  |                             |
| $I_{xcc} = I_{zcc}$  |  | 0.005144 kg m <sup>2</sup>  |
| $I_{yyc}$  |  | 0.0000487 kg m <sup>2</sup> |
| Inertia of piston and piston rod of prismatic link   |  |                             |
| $I_{xpp} = I_{zpp}$  |  | 0.00168 kg m <sup>2</sup>   |
| $I_{ypy}$  |  | 0.000025 kg m <sup>2</sup>  |
| Stiffness of spring in compliant link ( $k_f$ )  |  | 5000 N/m                    |
| Friction between the piston and cylinder of a prismatic link ( $R_f$ )   |  | 274 N s/m                   |
| Contact point stiffness at the piston cylinder of prismatic link ( $k_b$ )   |  | $10^8$ N/m                  |
| Contact point resistance at the piston and cylinder of prismatic link ( $R_b$ )  |  | $10^3$ N s/m                |
| Length of piston and piston rod of prismatic link $l_p$  |  | 0.1 m                       |
| Distance of cylinder CG from a cylinder end frame of a prismatic link ( $l_{cg}$ )                                     |  | 0.05 m                      |
| Distance of piston CG from a piston end frame of a prismatic link ( $l_{pg}$ )   |  | 0.07 m                      |
| Mass of piston & piston rod of the prismatic link ( $m_p$ )  |  | 0.2 kg                      |
| Mass of cylinder part of the prismatic link ( $m_c$ )  |  | 0.3 kg                      |
| Position of the cylinder end point with respect to the body fixed frame at the mass center in meter, $(x_2, y_2, z_2)$ |  | (0.0, -0.05, 0.0)           |
| Position of the piston end point with respect to the body fixed frame at the mass center in meter, $(x_3, y_3, z_3)$   |  | (0.0, 0.07, 0.0)            |
| <i>Common parameter</i>  |  |                             |
| Mass of body( $M_b$ )  |  | 6.94 kg                     |
| Inertia of Body  |  |                             |
| $I_{xb}$   |  | 0.1470 kg m <sup>2</sup>    |
| $I_{yb}$   |  | 0.1045 kg m <sup>2</sup>    |
| $I_{zb}$   |  | 0.2466 kg m <sup>2</sup>    |
| Ground damping in $x, y, z$ direction ( $R_{gx}, R_{gy}, R_{gz}$ )   |  | 1000 N s/m                  |
| Ground stiffness in $z$ direction ( $K_{gz}$ )   |  | $10^6$ N/m                  |
| <i>Controller parameter</i>  |  |                             |
| Proportional gain of controller ( $K_p$ )  |  | 100                         |
| Derivative gain of controller ( $K_V$ )  |  | 80                          |
| Integral gain of controller ( $K_I$ )  |  | 50                          |
| <i>Actuator parameter</i>  |  |                             |
| Motor constant ( $K_m$ )   |  | 0.0276 N m/A                |
| Motor armature resistance ( $R_m$ )  |  | 0.386 Ohms                  |
| Motor inductance ( $L_m$ )   |  | 0.001 H                     |
| Gear ratio ( $n$ )   |  | 230                         |

## References

- [1] D.J. Todd, Walking Machines, An Introduction to Legged Robots, Koran Page, London, 1985.
- [2] M.H. Raibert, Legged Robots That Balance, MIT Press, Cambridge, MA, 1986.
- [3] A. Sprowitz, A. Tuleu, M. Vespignani, M. Ajallooeian, E. Badri, A.J. Ijspeert, Towards dynamic trot gait locomotion design control and experiments with cheetah-cub, a compliant quadruped robot, *Int. J. Robot. Res.* 0 (0) (2013) 1–19.
- [4] K.C. Galloway, J.C. Clark, D.E. Koditschek, Variable stiffness legs for robust, efficient, and stable dynamic running, *J. Mech. Robot.* 5 (2013) (011009-1) –(011009-11).
- [5] J.M. Hollerbach, A recursive Lagrangian formulation of manipulator dynamics and a comparative study of dynamics formulation complexity, *IEEE Trans. Syst. Man Cybern.* 10 (11) (1980) 730–736.
- [6] W.W. Armstrong, Recursive solution of the equations of motion of an  $n$ -link manipulator, in: Proc. Fifth World Congress on the Theory of Machines and Mechanisms, Montreal, Canada, vol. 2, 1979, pp. 1342–1346.
- [7] M.W. Walker, D.E. Orin, Efficient dynamic computer simulation of robotic mechanisms, *J. Dyn. Syst. Meas. Contr.* 104 (1982) 205–211.
- [8] K.S. Anderson, Recursive derivation of explicit equations of motion for efficient dynamic/control simulation of large multibody systems (Ph.D. dissertation), Stanford University, 1990.
- [9] D.E. Rosenthal, An order n formulation for robotic systems, *J. Astronaut. Sci.* 38 (4) (1990) 511–529.
- [10] A.K. Banerjee, Block-diagonal equations for multibody elastodynamics with geometric stiffness and constraints, *J. Guid. Control Dyn.* 16 (6) (1993) 1092–1100.
- [11] D.S. Bae, E.J. Haug, A recursive formulation for constrained mechanical system dynamics: Part I. Open loop systems, *Mech. Struct. Mach.* 15 (3) (1987) 359–382.
- [12] M. Bennani, F. Giri, Dynamic modelling of a four legged robot, *J. Intell. Robot. Syst.* 17 (1996) 419–428.
- [13] A. Mahapatra, S.S. Roy, Computer aided dynamic simulation of six legged robot, *Int. J. Recent Trends Eng.* 2 (2) (2009) 146–151.
- [14] V.L. Krishnan, P.M. Pathak, L. Sardana, S.C. Jain, Simulation and experimental studies on walking robot with flexible legs, in: Proceeding of 4th International Conference on Integrated Modeling and Analysis in Applied Control and Automation, IMACA 2010, Fes, Morocco, 2010, pp. 11–19.
- [15] S. Soyguder, H. Ali, Computer simulation and dynamic modeling of a quadrupedal pronging gait robot with SLIP model, *Comput. Electr. Eng.* 28 (2012) 161–174.
- [16] S.V. Shah, S.K. Saha, J.K. Dutt, Modular framework for dynamic modeling and analyses of legged robots, *Mech. Mach. Theory* 49 (2012) 234–255.
- [17] K. Ganesh, P.M. Pathak, Dynamic modelling & simulation of a four legged jumping robot with compliant legs, *Robot. Auton. Syst.* 61 (2013) 221–228.
- [18] M.M. Gor, P.M. Pathak, A.K. Samantaray, J.-M. Yang, S.W. Kwak, Control of compliant legged quadruped robots in the workspace, *Simulation: Trans. Soc. Model. Simul. Int.* 91 (2) (2015) 103–125.
- [19] M.M. Gor, P.M. Pathak, A.K. Samantaray, J.-M. Yang, S.W. Kwak, Dynamic modeling and simulation of compliant legged quadruped robot, in: Proceedings of the 1st International and 16th National Conference on Machines and Mechanisms, iNaCoMM2013, IIT Roorkee, India, 18–20 December 2013, pp. 7–16.
- [20] X. Chen, F. Gao, C. Qi, X. Zhao, Spring parameters design to increase the loading capability of a hydraulic quadruped robot, in: Proceeding of the 2013 International conference on Advanced Mechatronics Systems, Luoyang, China, 2013, pp. 535–540.
- [21] M. Raibert, K. Blankenspoor, G. Nelson, R. Playter, BigDog, The rough terrain quadruped robot, in: 17th IFAC World Congress, COEX, South Korea, 2008, pp. 10823–10825.
- [22] A. Spröwitz, A. Tuleu, M. Vespignani, M. Ajallooeian, E. Badri, A.J. Ijspeert, Towards dynamic trot gait locomotion: Design, control, and experiments with Cheetah-cub, a compliant quadruped robot, *Int. J. Robot. Res.* 32 (8) (2013) 932–950.
- [23] C. Semini, N.G. Tsagarakis, E. Guglielmino, M. Focchi, F. Cannella, D.G. Caldwell, Design of HyQ—a hydraulically and electrically actuated quadruped robot, *Proc. Inst. Mech. Eng. Part I: J. Syst. Control Eng.* 225 (6) (2011) 831–849.
- [24] K. Byl, Metastable legged-robot locomotion (Ph.D. thesis), Massachusetts Institute of Technology, US, 2008.
- [25] A. Shkolnik, M. Levashev, I.R. Manchester, R. Tedrake, Bounding on rough terrain with the LittleDog robot, *Int. J. Robot. Res.* 30 (2011) 192–215.
- [26] Y. Fukuoka, H. Kimura, Dynamic locomotion of a biomorphic quadruped ‘Tekken’ robot using various gaits: walk, trot, free-gait and bound, *Appl. Bionics Biomech.* 6 (2009) 63–71.
- [27] H. Kimura, Y. Fukuoka, Biologically inspired adaptive dynamic walking in outdoor environment using a self-contained quadruped robot: ‘Tekken2’, in: 2004 IEEE/RSJ International Conference on Intelligent Robots and Systems, 2004, (IROS 2004), Proceedings. 2004, pp. 986–991.
- [28] C.D. Remy, M. Hutter, M. Hoepflinger, M. Bloesch, C. Gehring, R. Siegwart, Quadrupedal robots with stiff and compliant actuation, *Att-Automatisierungstechnik* 60 (11) (2012) 682–691.
- [29] D.C. Karnopp, D.L. Margolis, R.C. Rosenberg, System Dynamics: Modeling and Simulation of Mechatronic Systems, fourth ed., John Wiley & Sons, 2006.
- [30] R. Merzouki, A.K. Samantaray, P.M. Pathak, B. Ould Bouamama, Intelligent Mechatronic Systems—Modeling, Control and Diagnosis, Springer-Verlag, London, 2013.
- [31] J.J. Craig, Introduction to Robotics Mechanics and Control, third ed. Pearson Education, 2005.
- [32] T.K. Bera, A.K. Samantaray, R. Karmakar, Bond graph modeling of planar prismatic joint, in: Proc. 14th National Conf. Machines and Mechanisms, NaCoMM-09, Durgapur, India, December 17–18, 2009, pp. 22–26.
- [33] T. Ersal, H.K. Fathy, J.L. Stein, Structural simplification of modular bond-graph models based on junction inactivity, *Simul. Modell. Pract. Theory* 17 (2009) 175–196.
- [34] T.K. Bera, A.K. Samantaray, R. Karmakar, Bond graph modeling of planar prismatic joints, *Mech. Mach. Theory* 49 (2012) 2–20.
- [35] T.K. Bera, R. Merzouki, B.O. Bouamama, A.K. Samantaray, Force control in a parallel manipulator through virtual foundations, *Proc. Inst. Mech. Eng., Part I: J. Syst. Control Eng.* 226 (8) (2012) 1088–1106.
- [36] A.K. Ghosh, A. Mukherjee, M.A. Faruqi, Computation of driving efforts for mechanisms and robots using bond graphs, *Trans. ASME J. Dyn. Syst. Meas. Control* 113 (4) (1991) 744–748.
- [37] P.M. Pathak, A. Mukherjee, A. Dasgupta, Impedance control of space robots using passive degrees of freedom in controller domain, *Trans. ASME J. Dyn. Syst. Meas. Control* 127 (4) (2005) 564–578.
- [38] A.K. Samantaray, A. Mukherjee, User manual of SYMBOLS, High Tech. Consultants, STEP, Indian Institute of Technology, Kharagpur, 2000.
- [39] R.McN. Alexander, The gaits of bipedal and quadrupedal animals, *Int. J. Robot. Res.* 3 (2) (1984) 49–59.
- [40] G. Gabrielli, Th. von Karman, What price speed? Specific power required for propulsion of vehicles, *Mech. Eng.* 72 (10) (1950) 775–781.
- [41] P. Gregorio, M. Ahmadi, M. Buehler, Design, control, and energetics of an electrically actuated legged robot, *IEEE Trans. Syst. Man Cybern.* 27 (4) (1997) 626–634.
- [42] B. Siciliano, O. Khatib (Eds.), Springer Handbook of Robotics, Springer, 2008.
- [43] A.K. Samantaray, B. Ould Bouamama, Model-Based Process Supervision, Springer, 2008.
- [44] R.F. Ngwompo, S. Scavarda, Dimensioning problems in system design using bicausal bond graphs, *Simul. Pract. Theory* 7 (5–6) (1999) 577–587.



**M.M. Gor** received the B.E. and M.E. degree from B.V. Mahavidyalaya, V.V. Nagar, India in 2000 and 2008 respectively. He is faculty member of Department of Mechanical Engineering at G.H. Patel College of Engineering & Technology, V.V. Nagar, India. Currently he is pursuing his Ph.D. from the Department of Mechanical and Industrial Engineering, Indian Institute of Technology, Roorkee, India. He is working on dynamic modeling and control of walking robot.



**P.M. Pathak** received the B.Tech. degree in 1988 from NIT, Calicut, India and M.Tech. degree in 1998 from IIT, Kanpur, India. He received Ph.D. degree in 2005 from IIT, Kharagpur, India. Currently he is an Associate Professor in the Department of Mechanical and Industrial Engineering, Indian Institute of Technology, Roorkee, India. His research areas are Robotics, Dynamics, Control, Bond graph modeling, Design. Currently he is working on application areas of space robotics, underwater robotics, walking robot dynamics, mechatronics modeling and control. He has been active in these areas since last 13 years. He has published more than 35 research articles in reputed journals.



**A.K. Samantaray** graduated in 1989 from the College of Engineering and Technology (CET), India, in Mechanical Engineering. He received the master degree in Machine Dynamics and Ph.D. degree in Mechanical Engineering (Rotor Dynamics) from the Indian Institute of Technology (IIT)—Kharagpur, in 1991 and 1996, respectively. From 1996 to 2001, he worked as a Project Manager for High-Tech Consultants. From 2001 to 2004, he was a research scientist at Ecole Polytechnique de Lille, Université des Sciences et Technologies de Lille (France) and thereafter; he joined as a faculty member in the Department of Mechanical Engineering at the Indian Institute of Technology, Kharagpur. Currently, he is a full professor at IIT Kharagpur. He is the author of bond graph modeling software SYMBOLS. His research areas are multi-body dynamics, non-linear mechanics, and systems and control. He has authored three books, four book chapters, and more than 50 journal articles in his field. He is also a consultant to various industries requiring help in modeling, simulation, design, and automation.



**J.-M. Yang** received the B.S., M.S., and Ph.D. degrees in Electrical Engineering from Korea Advanced Institute of Science & Technology (KAIST), Korea, in 1993, 1995, and 1999, respectively. Currently he is an Associate Professor in Electrical Engineering Department of Kyungpook National University, Daegu, South Korea. His research interests are in gait study of walking machines and control of asynchronous sequential machines.



**S.W. Kwak** received his B.S., M.S., and Ph.D. degrees in Electrical Engineering from Korea Advanced Institute of Science & Technology (KAIST), Korea, in 1993, 1995 and 2000, respectively. Currently he is an Associate Professor in Department of Electrical Engineering, Keimyung University, Korea. His research interests are in control of asynchronous sequential machines, space-borne digital electronics, and fault-tolerance in real time systems.